Zeitschrift: IABSE reports of the working commissions = Rapports des commissions de travail AIPC = IVBH Berichte der Arbeitskommissionen

Band: 33 (1981)

Rubrik: Session 1: Modelling of material behaviour

Session 1

Modelling of Material Behaviour

Leere Seite
Blank page
Page vide

Advances in Deformation and Failure Models for Concrete

Développement dans le domaine des modèles de déformation et de rupture pour le béton

Entwicklungen auf dem Gebiete der Verformungs- und Bruchmodelle für Beton

ZDENĚK P. BAŽANT
Professor of Civil Engineering
Northwestern University
Evanston, IL, USA

SUMMARY

Presented is a non-exhaustive survey of recent advances in mathematical models for nonlinear multiaxial deformation of concrete, the short-time viscoelastic effects, the deformations due to cracks, the overall deformation of cracked concrete and the propagation of crack bands. Emphasis is placed on the treatment of fundamental phenomena such as internal friction and dilatancy due to shear, the interlocking of crack surfaces, and the propagation of crack bands. A new model for the strain-rate effect is presented. Numerical applications are discussed, especially for finite element analysis, and illustrative examples are cited.

RESUME

L'article présente les récents développements des modèles mathématiques pour les déformations non-linéaires et multiaxiales du béton, les effets visco-élastiques instantannés, l'influence des fissures sur les déformations, l'état de déformation en stade fissuré et le développement des zones fissurées. L'accent est mis sur le traitement des phénomènes fondamentaux comme la friction interne et le glissement dû au cisaillement, l'imbrication des surfaces de fissuration et le développement des zones fissurées. Un nouveau modèle pour l'influence de la vitesse des allongements sur les contraintes est également présenté. Des applications numériques, concernant plus spécialement l'analyse par les éléments finis, sont aussi discutées et quelques exemples présentés.

ZUSAMMENFASSUNG

In diesem Beitrag wird ein Überblick über die neuesten Entwicklungen mathematischer Modelle für das nichtlineare, mehrachsige Verformungsverhalten von Beton gegeben: das viscoelastische Kurzzeitverhalten, der Einfluss der Risse auf die Verformungen, der Verformungszustand in einem gewissen Stadium. Es wird im besonderen eingegangen auf einige grundlegende Probleme, wie die innere Reibung und Schiebung infolge Scherkraft, die Verzahnung von Rissequerschnitten und die Ausbreitung von Rissezonen. Ein neues Modell für das Spannungs-Dehnungs-Zeit-Verhalten wird vorgestellt. Anschliessend werden kurze Anwendungsbeispiele numerisch durchgerechnet und erläutert, insbesondere im Hinblick auf eine Behandlung mittels finiter Elemente.

1. INTRODUCTION

At the present time we are witnessing rapid advances in the mechanics of concrete structures. We are discovering general laws governing the behavior of these structures and building mathematical models to predict this behavior. The subject is being placed on a firm scientific basis. The reason for this development is two-fold: first, more realistic and more accurate predictions of structural performance are needed to improve the safety, serviceability and economy of the structures as well as to enable safe and economic design of new types of concrete structures such as nuclear reactor vessels and containments, ocean structures, very large span bridges and very tall buildings, etc; second, we must recognize that this development is being stimulated and in fact made possible by the availability of powerful computation tools, especially the finite element method. Without the availability of these tools, which was the situation not so long ago, development of sophisticated models for concrete structures would have been practically useless.

Significant advances have recently been made in various directions including (a) nonlinear triaxial models for solid concrete, (b) fracture of concrete and behavior of cracked concrete, (c) concrete creep, (d) thermal effects, (e) moisture effects, (f) chemical effects and corrosion, (g) probabilistic aspects. The spectrum of recent developments in these subjects is too broad to permit their exposition in a single lecture. Therefore, we must limit our scope and we will concentrate our attention to nonlinear triaxial behavior and cracking. In a little more detail we will treat the question of strain-rate effect and short-time viscoelasticity in triaxial deformation, in order to use this opportunity to present some known results not yet published.

No claims for the completeness of the present survey are made. In fact, the survey which follows is rather selective and emphasizes the contributions in which the writer was directly involved or with which he is closely familiar. These are mostly the contributions made at Northwestern University and also some made at Argonne National Laboratory.

2. NONLINEAR TRIAXIAL BEHAVIOR OF SOLID CONCRETE

2.1. Friction and Dilatancy

Friction is one of the most difficult features in constitutive modeling. It leads to violation of the basic stability postulate, namely Drucker's postulate [1-4], which serves as the basis for the flow rule of incremental plasticity (normality rule). This postulate is expressed by the condition

$$\Delta W = \frac{1}{2}\, d\sigma_{ij} d\epsilon_{ij}^{p\ell} > 0 \qquad (1)$$

in which ΔW represents the dissipated second order work during a cycle of applying and removing stress increments $d\sigma_{ij}$, and $d\epsilon_{ij}^{p\ell}$ are the increments of plastic strains. This postulate is known to constitute a sufficient but not necessary condition for local stability of the material.[1] Thus, its violation does not necessarily imply instability, which is a fact often forgetten by numerical analysts, many of whom insist on using numerical models with symmetric equation systems which are guaranteed if the postulate is satisfied. It has been, however, shown [e.g., 15] that inequality (1) may be violated due to internal friction without causing an instability of the material. It is, therefore of considerable interest to find a more general inequality which indicates

[1] See [1, 2, 15, 16, 18]

the admissible stable frictional deformations. It has recently been found [5] that the material is stable if the following inequality

$$\Delta W - \chi \Delta W_f > 0 \tag{2}$$

is satisfied for any value of χ between 0 and 1; $0 \le \chi \le 1$. Here ΔW_f represents what can be called a frictionally blocked elastic energy, expressed as

$$\Delta W_f = \frac{\beta' - \beta^*}{2C} d\sigma (d\bar{\tau} + \beta^* d\sigma) \tag{3}$$

in which C, β' and β^* are expressed in terms of the loading function. Although the expressions for a completely general loading function are possible [5], we consider loading functions of the form [27]

$$F(\sigma, \bar{\tau}, \hat{\gamma}^{p\ell}) = 0 \tag{4}$$

in which σ represents the mean (hydrostatic) stress, $\sigma = \sigma_{kk}/3$; $\bar{\tau}$ = stress intensity = $(e_{ij}e_{ij}/2)^{\frac{1}{2}}$ where e_{ij} = deviator of strain tensor ϵ_{ij}; and $\hat{\gamma}^{p\ell}$ = length of the path traced in the space of plastic strains, which is used as a hardening parameter. Tensorial subscripts refer to cartesian coordinates x_i ($i = 1,2,3$) and repetition of subscripts implies summation. The constants in Eq. 3 are now expressed as [5]:

$$C = -k_1 \frac{\partial F/\partial \hat{\gamma}^{p\ell}}{\partial F/\partial \bar{\tau}}, \qquad \beta' = \frac{\partial F/\partial \sigma}{\partial F/\partial \bar{\tau}}, \qquad \beta^* = k_2 \frac{d\epsilon^{p\ell}}{d\hat{\gamma}^{p\ell}} \tag{5}$$

Their meaning may be illustrated taking recourse to Mandel's example [15] (Fig. 1) of a frictional block resting on a rough surface, loaded by a vertical force simulating hydrostatic stress σ, and also subjected to force F from a horizontal spring such that the sliding of the block is imminent. An applied horizontal force on the block simulates $d\bar{\tau}$. Mandel showed that if a disturbing force $d\sigma_{ij}$ inclined from the vertical to the left by an angle less than the friction angle is applied, a sliding of the block results but the block remains stable because it slides only an infinitesimal distance to the right. Yet, Drucker's postulate (Eq. 1) is violated for this movement. Inequality (2) is, however, not violated and coefficient C from this inequality (Eq. 3) represents the spring constant, coefficient β' is the friction coefficient of the block, and β^* is the dilatancy angle indicating the ratio of lifting of the block to its sliding. Coefficients k_1 and k_2 in Eq. 5 are not illustrated by this example and depend on the direction of loading in stress and strain spaces [5].

The usefulness of the new, more general condition sufficient for material stability (Eqs. 2,3) is that it is possible to formulate a frictional constitutive relation and check whether it guarantees stability. Furthermore, by pursuing the same line of reasoning as in classical incremental plasticity, one can derive the flow rule associated with this inequality. It appears that this flow rule allows certain, but not arbitrary, violations of normality of the plastic strain increment vector to the current loading surface. For example it is found [5] that in the plane of $\bar{\tau}$ versus σ the admissible load increment vectors can deviate from the normal to the right and fill a fan of directions, the limiting inclined direction being uniquely determined by the loading surface. The resulting flow rule is, however, totally different from non-associated plasticity because a single loading surface is used and because, in contrast to non-associated plasticity, stability of the material is guaranteed,

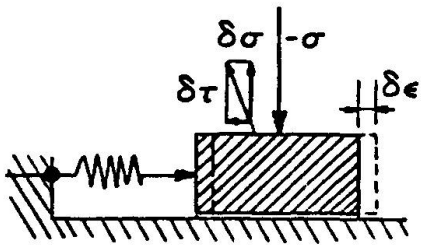

Fig. 1 Example of Spring Loaded Frictional Block

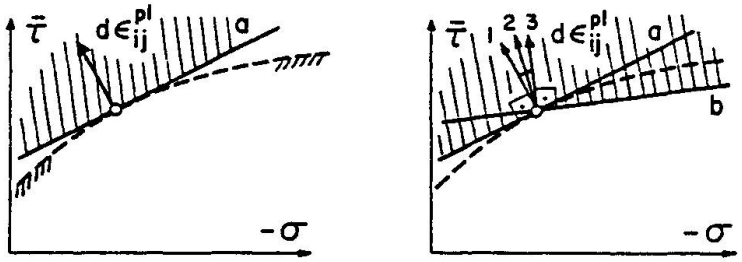

Fig. 2 Plastic Strain Increment Relative to Loading Surface [5]

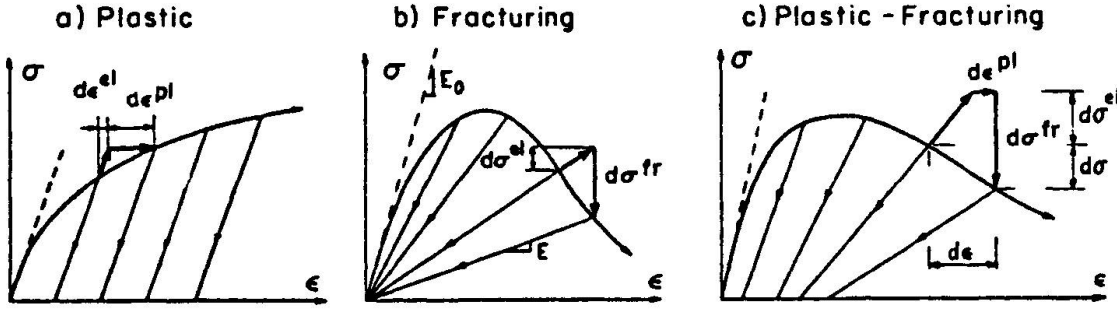

Fig. 3 Characteristic Unloading Behavior

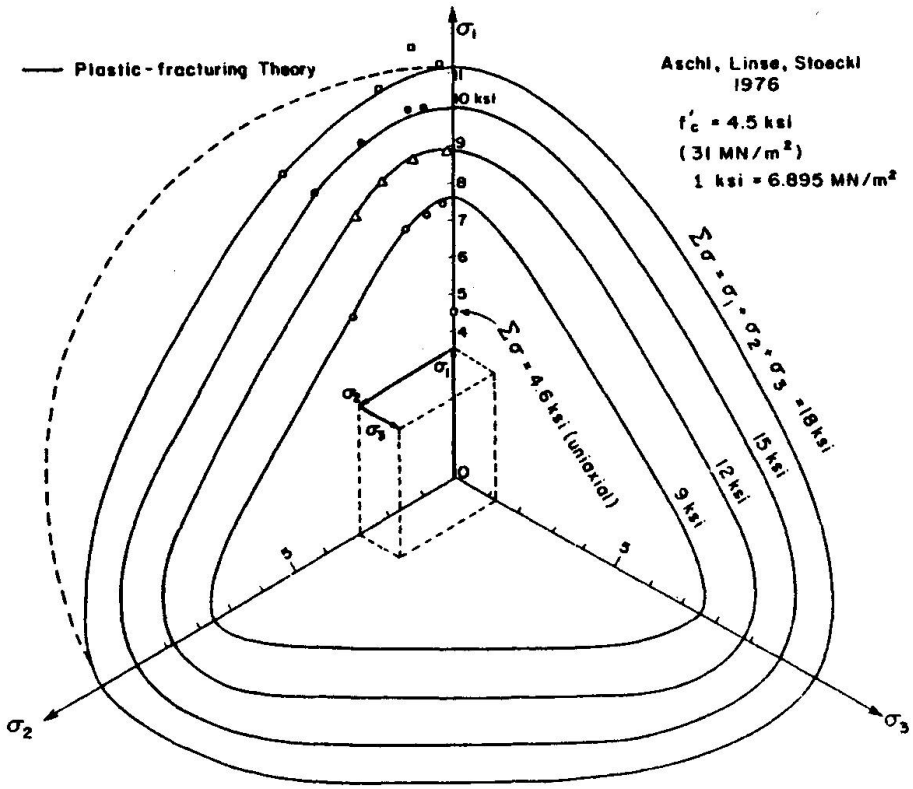

Fig. 4 Failure Envelopes for Plastic-Fracturing Theory whose Loading Surface Does not Involve Third Invariants

and also becuase the limiting inclined direction of the fan (Fig. 2) depends on the previous loading history and the hardening or softening properties of the material.

Inequality (2) involves only the friction in deviatoric shear due to hydrostatic compressive stress. It is possible to obtain a still more general inequality [5] which also involves the friction in volume change due to deviatoric shear stress, a phenomenon which was termed the inverse friction. Further generalizations of the frictional phenomena, the sufficient stability condition, and the corresponding flow rule are possible by considering frictional phenomena in fracturing stress relaxations, to which we now turn our attention.

2.2 Plastic-Fracturing Theory

Plastic-fracturing theory is a recent extension of classical incremental plasticity [6] which adheres to the use of loading surfaces and flow rule based on these surfaces, and introduces, in addition to plastic strain increments, the fracturing stress relaxations due to micro-fracturing (micro-cracking). The extension to model the inelastic phenomena due to micro-cracking appears to be essential for materials such as concrete as well as rocks. The nature of the theory may be illustrated by Fig. 3, in which plasticity is seen to be characterized by an elastic increment followed by a horizontal plastic strain increment. A material which undergoes only micro-fracturing and no plastic deformation, first studied by Dougill [13,14], is shown in Fig. 3b where the elastic increment is followed by a vertical fracturing stress decrement. While plasticity obviously does not allow strain-softening, i.e., decline of stress at increasing strain, the fracturing theory does. To be able to distinguish strain softening from unloading, the loading surfaces for the fracturing theory must be considered as functions of strains rather than stresses, as was first done by Dougill [13,14], who also introduced the normality rule in the strain space to obtain fracturing stress relaxations. The plastic-fracturing theory is a combination of plastic and fracturing theories and is illustrated in Fig. 3c, where the elastic increment is followed by a horizontal plastic strain increment and then by a vertical fracturing stress decrement. Obviously, the strain softening is also allowed for this theory. The plastic strain increments and fracturing stress decrements are then obtained on the basis of separate loading surfaces in the stress and strain spaces. The characteristic property which allows us to distinguish between plastic and fracturing phenomena is the unloading slope. The plastic phenomena do not lead to any change in the unloading stiffness, while the fracturing phenomena are totally related to a change in the unloading stiffness, and in case of pure fracturing behavior, they preserve total reversibility at complete unloading, as indicated by the fact that the unloading slope in Fig. 3b shoots to the origin. In plastic-fracturing materials (Fig. 3c) the unloading slope decreases but does not point to the origin. If unloading slope is known for each point of the loading diagram, it is possible to uniquely separate the plastic and fracturing effects [see 5].

The plastic-fracturing theory leads to the following incremental stress-strain relations [6]

$$ds_{ij} = 2G\, de_{ij} - 2G\, s_{ij} \frac{d\mu}{\bar{\tau}} - e_{ij} \frac{d\varkappa}{\bar{\gamma}} \tag{6}$$

$$d\sigma = 3K\, d\varepsilon - 2K\beta\, d\mu - \frac{2}{3}\alpha\, d\varkappa \tag{7}$$

in which

$$d\varkappa = H_1 (d\bar{\gamma} + \alpha' d\epsilon) \tag{8}$$

$$d\mu = H_2 (G\, s_{km}\, de_{km} + \bar{\tau} K \beta' d\epsilon_{kk}) \tag{9}$$

Here G = elastic shear modulus, K = elastic bulk modulus (both variable); s_{ij} = deviator of stress tensor σ_{ij}, e_{ij} = deviator of strain tensor ϵ_{ij}, σ = mean stress, ϵ = mean (volumetric) strain = $\epsilon_{kk}/3$; $\mu, \varkappa$ = parameters for plastic and fracturing hardening and softening; $\bar{\tau}$ = stress intensity, $\bar{\gamma}$ = strain intensity = $(e_{ij}e_{ij}/2)^{\frac{1}{2}}$; β', α' = plastic and fracturing internal friction coefficients; β, α = plastic and fracturing dilatancy factors giving the ratio of volumetric to deviatoric inelastic increments; and H_1, H_2 = hardening and softening stiffnesses. The inelastic response is here totally characterized by six coefficients, H_1, H_2, β', α', β, α, the dependence of which on the invariants of stress and strain must be determined from experiment. Various other considerations are needed for this purpose and suitable functions for these coefficients have been identified, leading to a rather close agreement with a broad range of experimental data available in the literature [see 6].

In contrast to incremental plasticity, the constitutive equations of plastic-fracturing theory (Eqs. 6-9) involve not only terms which depend on stress (the term with s_{ij} in Eq. 6), but also terms which depend on strains such as the term involving e_{ij} in Eq. 6. These terms appear to be very helpful in representing material behavior in strain-softening regimes, which is due simply to the fact that e_{ij} increases during strain-softening while s_{ij} decreases. These strain-dependent terms give rather different lateral strains and thus allow us to model the large volume dilatancy during strain-softening. Another essential difference from plasticity is that the shear and bulk elastic moduli are variable. As mentioned, their decrease is tied to the growth of fracturing parameter $\varkappa$, for which the following equations were obtained:[2]

$$dG = -\frac{d\varkappa}{2\bar{\gamma}} \qquad dK = -\frac{2\alpha}{9}\,\frac{d\varkappa}{\epsilon} \tag{10}$$

It should be also observed that Eqs. 8, 9 apply only to loading; for unloading modified expressions must be introduced. In analogy to plasticity, one might set $d\varkappa = d\mu = 0$, but then no representation of inelastic behavior on unloading, reloading and cyclic loading would be possible. It is possible, however, to formulate rules which allow for nonzero $d\varkappa$ and $d\mu$ during unloading and cyclic loading [21,5]. These rules consist in the so-called jump-kinematic hardening, in which the center of the loading surface is jumped to the last extreme stress or strain point whenever loading is reversed to unloading or vice versa. Three-way loading-unloading-reloading criteria are needed for this purpose [21,5].

The most important advantage of the plastic-fracturing theory is the fact that the stress-strain relations (Eqs. 6-9) can be brought (for loading) to an incrementally linear form:

$$d\sigma_{ij} = C_{ijkm}(\underset{\sim}{\sigma}, \underset{\sim}{\epsilon})\, de_{km} \tag{11}$$

$$\text{or} \quad d\underset{\sim}{\sigma} = \underset{\sim}{C}(\underset{\sim}{\sigma}, \underset{\sim}{\epsilon}) d\underset{\sim}{\epsilon} \tag{11a}$$

in which C_{ijkm} or $\underset{\sim}{C}$ represent the tensor or matrix of the tangential moduli

[2] See [26]

which are functions of the invariants of the stress tensor $\underset{\sim}{\sigma}$ and strain tensor $\underset{\sim}{\varepsilon}$; see Ref. 6. The use of tangential moduli is the most effective approach in step-by-step finite element analysis. It must be observed, however, that the matrix of tangential moduli is non-symmetric, which is a consequence of internal friction and is inevitable for close representation of experimental data on the material. This is certainly an inconvenience for numerical finite element analysis. However, it must be emphasized that this type of non-symmetry does not cause material instability as long as the new stability postulate in inequality (2) is satisfied. It should be also noted that tangential moduli C_{ijkm} have a generally anisotropic (non-isotropic and non-orthotropic) form, which is a manifestation of the stress- and strain-induced anisotropy.

The stress-strain relations in Eqs. 6-9 were derived by using loading surfaces that do not involve the third invariants of stress and strain. It is, however, interesting that the failure envelopes obtained from these relations (by recording the peaks of the stress-strain diagrams run at various ratios of stress components) have a form that is non-circular on the octahedral plane (π - projection). This is illustrated in Fig. 4, which was constructed from the numerical values of the coefficients of the plastic-fracturing theory from Ref. 6. This shows that the rounded triangular shape of the octahedral section does not necessarily imply the influence of the third stress invariant. This shape can equally well be caused by the simultaneous influence of stress and strain and the fact that these do not increase proportionally.

The plastic-fracturing theory has been shown to be capable of representing a very broad range of inelastic phenomena, including strain-softening, inelastic dilatancy due to shear and internal friction, as manifested by the great effect of hydrostatic compression in triaxial tests, the increase of volume in pre-peak as well as post-peak deformation, lateral strains, the increase of apparent Poisson's ratio, hysteretic loops during cyclic loading to small as well as high strain levels, etc. [23-25, 28-32].

2.3 Endochronic Theory

The central concept in the endochronic theory, first introduced by Valanis [8] although implied in various preceding works [e.g. 7], is that of intrinsic time, a variable which depends on the length ξ of the path traced by the states of the material in the strain space. A typical definition of intrinsic time, z, is:

$$dz = F_1(z, \underset{\sim}{\sigma}, \underset{\sim}{\varepsilon})d\xi, \qquad d\xi = \sqrt{\frac{1}{2}\, de_{ij} de_{ij}} \tag{12}$$

in which F_1 is a function of the stress and strain invariants and models the hardening or softening of the material during the evolution of inelastic strain. The inelastic strain increments are assumed to be proportional to small dz and the constitutive relation of endochronic theory is typified by the following:

$$de_{ij} = \frac{ds_{ij}}{2G} + \frac{s_{ij}}{2G}\, dz \tag{13}$$

$$d\epsilon = \frac{d\sigma}{3K} + d\lambda \tag{14}$$

Here an additional variable, $d\lambda$ [9], is introduced to model the inelastic volume dilatancy due to shear. It is also related to intrinsic time:

$$d\lambda = F_2(z,\underset{\sim}{\sigma},\underset{\sim}{\varepsilon})d\xi \tag{15}$$

It can be shown that the endochronic theory is a special case of viscoplasticity in which the viscosity coefficients depend not only on stress and strain but also on the strain rate [21,7]. The chief advantage of the endochronic theory, first recognized by Valanis is the fact that it is capable of representing the unloading irreversibility, the salient feature of inelastic behavior without the use of any inequalities (unloading criteria). This makes the endochronic theory extremely effective for cyclic loading. Furthermore, the fact that the inelastic strains are tied to one time-like variable dz makes it easy to control the stiffening or softening of the material by changing the rate of growth of the intrinsic time. One aspect which is represented well modeled by the theory is the inelastic volume dilatancy $d\lambda$.

The most significant difference of the endochronic theory from classical plasticity as well as plastic-fracturing theory is the fact that even for loading it can not be reduced to an incrementally linear form given by Eq. 11. Nevertheless, in the vicinity of any specified loading direction the endochronic theory can be linearized and put into this incrementally linear form [21]. However, the tangential moduli C_{ijkm} of this linearized form are not constant and depend on the chosen direction in the vicinity of which the behavior is linearized. It may seem that the lack of incrementally linear formulation would cause significant difficulties in numerical computation. However, finite element programs utilizing endochronic theory have been written [e.g., 10, 11, 12] and no particular convergence difficulties have been encountered.

Endochronic theories have recently been criticized from the viewpoint of material stability and uniqueness of response [19,20]. Subsequently, it was shown however, that the theory can be either modified to satisfy these requirements, for example by the use of jump-kinematic hardening and by unloading-reloading criteria [21,10], or that the strong uniqueness requirements are themselves in question. For example, Rivlin [20] pointed out that when one considers a staircase loading history in the strain space (Fig. 5) and when one lets the size of the stairs shrink to zero and their number go to infinity, the limiting behavior does not approach that for the smooth loading path. It is, however, possible to formulate a refined definition of intrinsic time for which the limit coincides [5], although at the same time the need for doing this may be questioned because the staircase loading path does not cause the same type of damage to the material as does the smooth loading path.

2.4 Further Comments

To exemplify the representation of inelastic behavior that can be obtained with the plastic-fracturing theory, we show some of the fits of test data[3] from Ref. 6 in Figs. 6,7. Just about equally good fits of material behavior have been obtained using the endochronic theory. One might wonder why two rather different theories allow representation of the same phenomena. The answer is that our information on the material behavior is far from complete and is insufficient to completely define the mathematical formulation. Therefore, certain logical assumptions must inevitably be used and the resulting formulation also depends on these. It appears that the most significant difference between various theories of inelastic behavior is obtained when a proportional loading is followed by sudden load increments to the side of the previous loading path; e.g., when an increase of normal stress is followed by a sudden shear stress increment. The different responses for such loading may be graphically illus-

[3] See [23-25, 28-32]

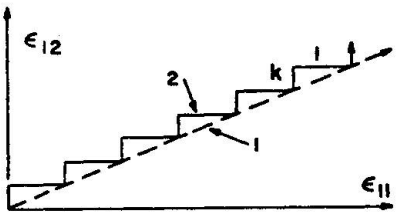

Fig. 5 Staircase Loading Path

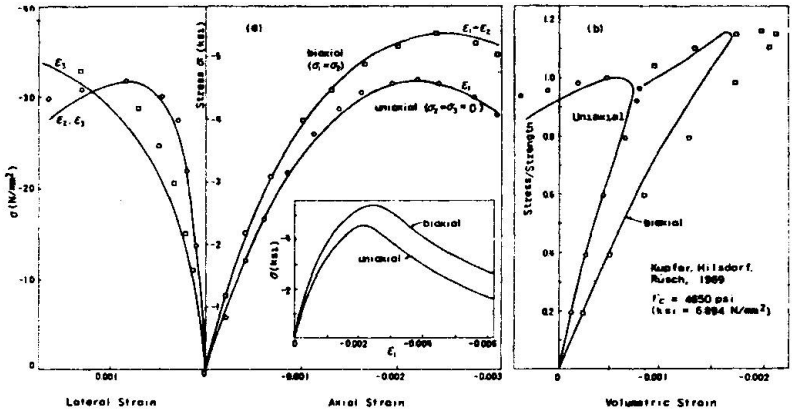

Fig. 6 Representation of Typical Published Uniaxial and Biaxial Test Data of Plastic-Fracturing Theory [6].

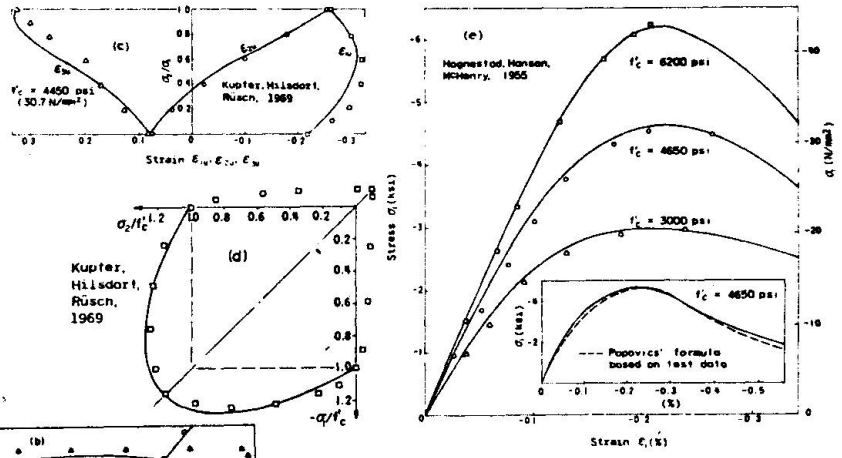

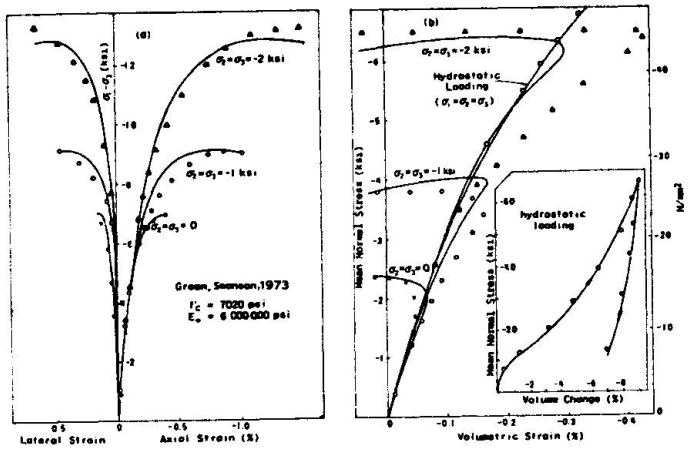

Fig. 7 Representation of Typical Published Triaxial Test Data of Plastic-Fracturing Theory [6]

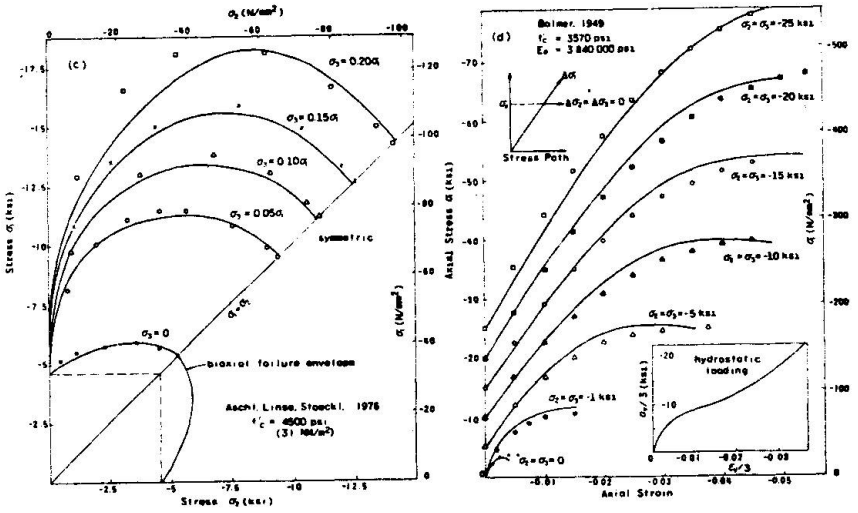

trated in terms of the inelastic stiffness locus [21]. It is unfortunately for such loading paths that measurements are most difficult and the present experimental information is rather scant. However, improvement of our knowledge for this type of loading is important because the loading "to the side" is characteristic of failures due to material instability.

Many other useful recent models for inelastic behavior of concrete have to be left out. Some of these are distinguished by greater simplicity compared to the models we considered. However, not all of the currently used models are in a correct form. For example, the so-called orthotropic models, in which the increments of strain and stresses are assumed to be related by a tangential moduli matrix of the same form as for an orthotropic material, violate the requirements of tensorial invariance, i.e., invariance of the formulation with regard to rotation of the chosen coordinate axes. [51,52,54]. One obtains with the orthotropic models different results depending on the orientation of the material coordinate axes in the initial state, which is inadmissible. The only way to avoid such spurious non-uniqueness is to rotate the material axes keeping them always oriented in the directions of principal stresses. However, rotation of material axes with regard to the material during the deformation is inadmissible, because it would imply that microcracks and other inelastic defects are rotated against the material. Consequently, the orthotropic models can work correctly only when the directions of principal stresses do not rotate [50], which is, however an unacceptable restriction for finite element programs. It should be observed that these difficulties cannot be detected with the so called true triaxial tests on cubical specimens since the principal stress directions in these tests remain always fixed. We now see that this type of testing has a serious limitation, although it does provide information on the effect of medium principal stress. We need to test the material under conditions of rotating principal stress directions, and further refinement of constitutive theories will have to be based on this type of testing. [50].

The failure conditions have been omitted in our preceding analysis. We take here the point of view that the failure condition for a material with a smooth evolution of response should be an integral part of the constitutive relation. Thus, under stress-controlled conditions the failure is obtained when strains can increase without any change in stress, which corresponds to the peak points of the stress-strain diagram as the failure condition. Under general conditions in which the stresses are not directly controlled the question of failure is more difficult and requires the analysis of stability, both local stability and overall stability of the structure. In such an approach, the stability analysis should in principle also determine ductility. For this purpose, one must analyze the so-called strain-localization instability, which consists in localization of uniformly distributed strain into a narrow band, a phenomenon which borders on fracture. Such analysis of ductility is easy (Figure 8) for a homogeneously stressed specimen, see [17,33], but gets much more difficult in general situations. The principle is not difficult: one must seek the point of singularity of the tangential stiffness matrix of the structure. What makes it difficult, and is normally disregarded in structural analysis, is the fact that there are many possible tangential stiffness matrices to be checked. Even when we consider classical plasticity we have for each finite element two possible stiffness matrices, one for loading and one for unloading. Now, in principle, one would have to check all possible combinations of finite element stiffnesses for loading and unloading from various elements which leads to a preposterously large number of stiffness matrices to be examined. The number of stiffness matrices to be checked gets even larger for theories which allow not just different stiffnesses for loading and unloading, but also for different directions

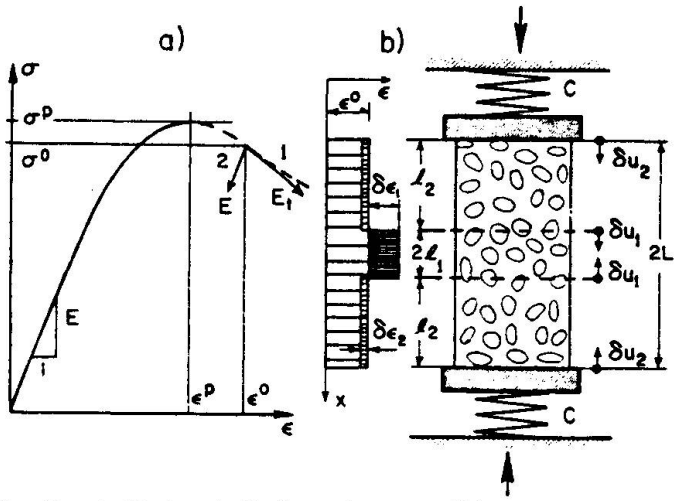

Fig. 8 Simplest Uniaxial Strain-Localization Instability due to Strain Softening

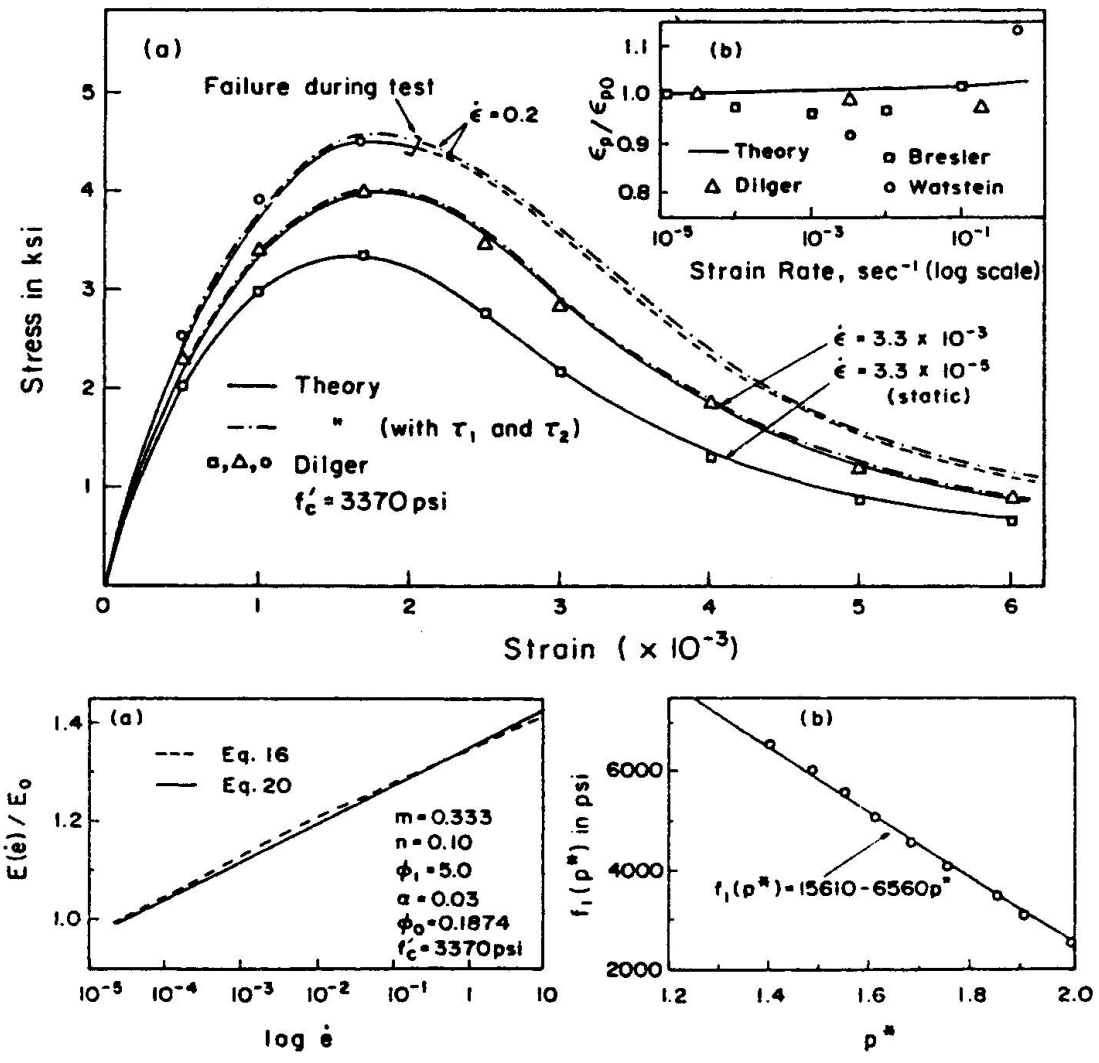

Fig. 9 Effect of Strain Rate on Stress-Strain Diagram, Compression Strength and Elastic Modulus (after [34])

of loading, especially for endochronic theory. For this reason, a different approach, namely that of fracture mechanics is inevitable for the determination of failure under general conditions. We must, however, keep in mind, and this is usually overlooked, that the non-singularity of the incremental stiffness matrix in finite element analysis does not signal stability and lack of failure for the analyst because he normally cannot check (and does not check) all possible incremental stiffness matrices.

3. SHORT-TIME VISCOELASTIC EFFECTS IN NONLINEAR TRIAXIAL DEFORMATION

3.1. Strain-Rate Effect

The triaxial constitutive equations are normally formulated on the basis of static loading tests in which failure is usually obtained within several minutes. However, for dynamic structural analysis it is necessary to consider strain rates which differ by several orders of magnitude. The strain rate is known to have a significant effect on the stiffness and strength of concrete and must, therefore, be introduced into the triaxial constitutive relations. We will now briefly outline a recently completed model [34] for the strain-rate effect.

The material parameters for the plastic-fracturing as well as endochronic theory were determined as a function of concrete strength f_c', which appears to be the main parameter affecting the shape of the response curves. Thus, the constitutive relation may be considered in the form:

$$d\sigma_{ij} = C_{ijkm}(\underset{\sim}{\sigma}, \underset{\sim}{\varepsilon};\ f_c')\ d\varepsilon_{km} \tag{16}$$

This equation, for example, models the fact that for a higher concrete strength the uniaxial response curve has a sharper peak and a steeper declining branch. The sharpness of the peak may conveniently be characterized by the parameter

$$p = \frac{E\varepsilon_p}{\sigma_p} \tag{17}$$

in which σ_p = peak stress and ε_p = strain at peak stress. The static behavior of concrete is to a large extent characterized by the values of elastic modulus E, peak stress (strength) σ_p, and parameter p. Under dynamic loading the values of these parameters are transformed to E*, σ_p*, p*, and one needs to determine how these parameters depend on the strain rate. The strain rate may of course independently affect other parameters of the response, but at present insufficient experimental information on the strain-rate effect in triaxial loading is available for using any more parameters. The foregoing three parameters may be controlled by replacing Eq. 16 with the equation:

$$b\, d\underset{\sim}{\sigma} = \underset{\sim}{C}\left(b\,\underset{\sim}{\sigma},\ a\,\underset{\sim}{\varepsilon};\ f_1(p^*)\right) a\, d\underset{\sim}{\varepsilon} \tag{18}$$

in which

$$b = \frac{f_1(p^*)}{\sigma_p^*}, \qquad a = \frac{E^*}{f_2(p^*)}\ b \tag{19}$$

Here functions $f_1(p^*)$ and $f_2(p^*)$ characterize the change of peak stress and initial elastic modulus. These functions may be determined by calculating uniaxial response curves from the plastic-fracturing theory equations and

plotting the obtained values of peak stress and elastic modulus against parameter p. In this manner, the following relations have been obtained [34]:

$$f_1(p^*) = (15610 - 6560\, p^*) \quad [\text{psi}] \tag{20}$$

$$f_2(p^*) = [0.9 + 0.00006\, f_1(p^*)]57000\sqrt{f_1(p^*)} \quad [\text{psi}] \tag{21}$$

in which f_1 and f_2 are in psi.

By analysis of numerous test data on the strain-rate effect, the dependence of p^* and σ_p^* on the strain rate was determined[34]:

$$p^* = 2.09 - 0.06 \log \dot{e} - 0.15\, \sigma_{p_0} \quad (\text{ksi}) \tag{22}$$

$$\sigma_p^* = \sigma_{p_0}(1.4 + 0.09 \log \dot{e}) \tag{23}$$

in which $\dot{e}$ represents the magnitude of the strain rate. Under triaxial strain situations this magnitude may be defined as a suitable invariant of the strain rate tensor, and the expression $\dot{e} = 0.9\,(\dot{\varepsilon}_{ij}\dot{\varepsilon}_{ij})^{\frac{1}{2}}$ has been used [34]. The effect of strain rate on the elastic modulus may be also deduced from the double power law for concrete creep, the validity of which appears to extend into very rapid loading. From that approach [48,49], it has been found that [34]

$$\frac{E^*}{E} = \frac{1 + (3.3 \times 10^{-6})^{-n}\varphi_0}{1 + (0.1\,\dot{e})^{-n}\varphi_0} \tag{24}$$

in which φ_0 and n are material constants. Using the foregoing expressions for p^*, E^*, σ_p^*, f_1 and f_2, the stress-strain relation acquires the form:

$$\dot{\sigma}_{ij} = C_{ijkm}(\underset{\sim}{\sigma}, \underset{\sim}{\varepsilon}, \dot{e})\ \dot{\varepsilon}_{km} \tag{25}$$

i.e., the tangential moduli are obtained as functions of not only the stress and strain invariants but also as functions of strain-rate magnitude $\dot{e}$.

3.2 Strain-Rate Effect with Rapid Creep and Relaxation

Eq. 25 introduces the strain-rate effect in a relatively simple form, but is incomplete because it can represent neither the increase of strain at constant stress (rapid creep) nor the decrease of stress at constant strain (rapid relaxation). To model all these short-time viscoelastic phenomena, a complete viscoelastic or visco-plastic formulation is inevitable. As the simplest complete viscoelastic model, one may use the first order differential equation:

$$\dot{\sigma}_{ij} + \frac{1}{\tau_1}\sigma_{ij} = C^e_{ijkm}\left(\dot{\varepsilon}_{km} + \frac{1}{\tau_2}\varepsilon_{km}\right) \tag{26}$$

in which C^e_{ijkm} are tangential moduli independent of the strain rate, and τ_1, τ_2 are the relaxation and retardation times. If the tangential moduli were constant, this equation would correspond to the well-known standard solid. It is known that the standard solid can describe the viscoelastic properties only within a relatively narrow range of time delays and time rates, roughly within one order of their magnitude. To avoid the complexities of using a model with a broad range of relaxation times, which necessitates higher order differential equations or integral equations [46], it has been proposed [34] to identify the

[45]

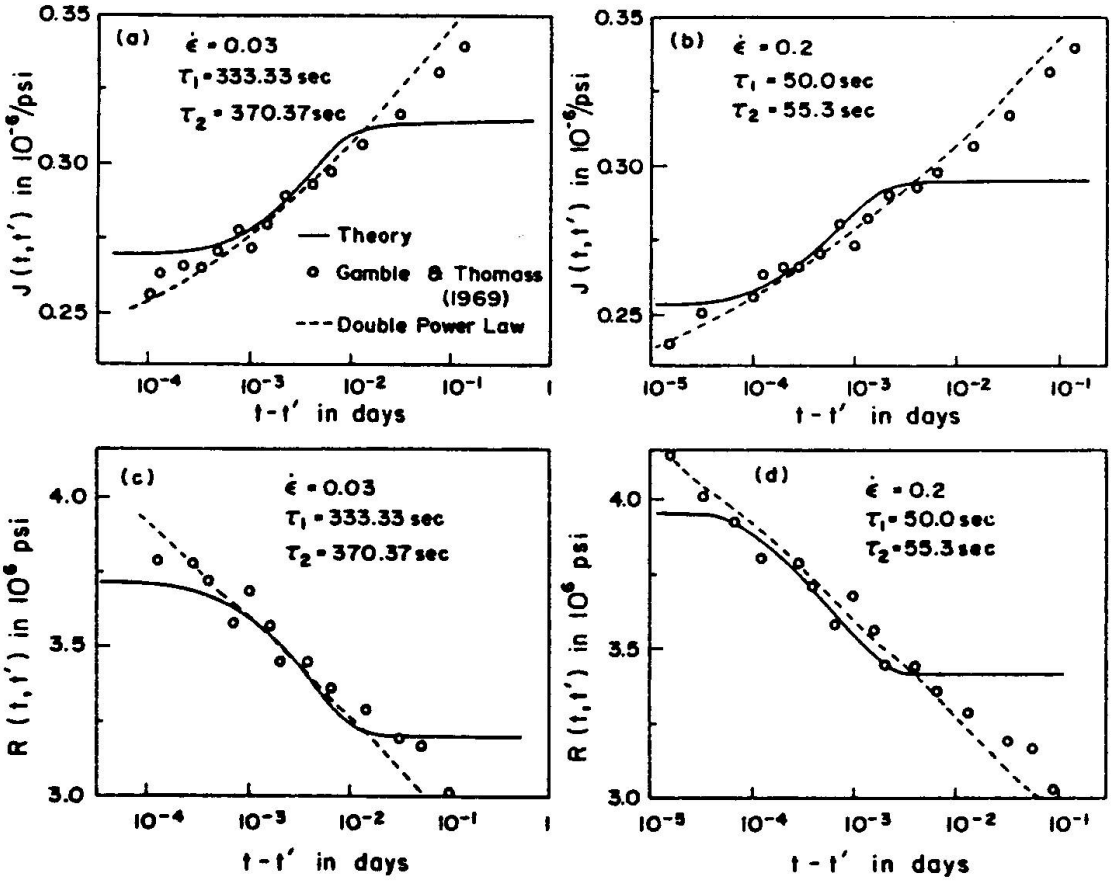

Fig. 10 Rapid Creep and Rapid Relaxation and Their Theoretical Representation from Ref. [34]

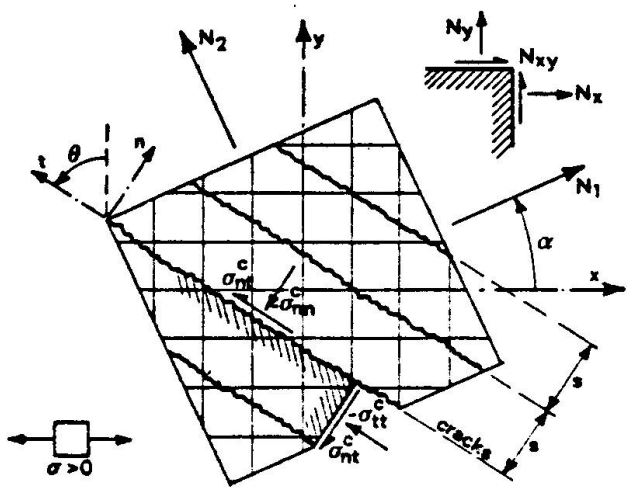

Fig. 11 Forces on the Cracks in Reinforced Concrete

parameters in Eq. 26 in such a manner that the response is closely approximated for the strain-rate magnitude $\dot{e}$ that is characteristic of the given dynamic problem, for example, the root-mean-square value $\langle\dot{e}\rangle$ of strain rate $\dot{e}$ over the time period of interest. One may then determine the parameters in this equation by fitting the corresponding response to various constant strain-rates to that predicted by the previous equation, Eq. 25, so as to obtain optimum approximation near the characteristic strain rate. The necessary calculations have been carried out and it was found that the following parameters give the desired approximation:

$$\tau_1 = (0.1\,\langle\dot{e}\rangle)^{-1} \text{ seconds} \tag{27}$$

$$E_1 = E(\dot{e}) + 1.39\, k_s \frac{dE(\dot{e})}{de}\,\dot{e} \tag{28}$$

$$\tau_2 = \frac{\tau_1 E_1}{2.72\,E(\dot{e}) - 1.72\,E_1} \tag{29}$$

$$C^e_{ijkm} = \frac{E_1}{E(\langle\dot{e}\rangle)}\; C_{ijkm}(\underset{\sim}{\sigma},\ \underset{\sim}{\varepsilon},\ \langle\dot{e}\rangle) \tag{30}$$

With the above parameters, Eq. 26 gives about the same strain-rate effect as Eq. 25, yet at the same time it gives short-time creep and relaxation.

Examples of some comparisons with test data available in the literature, which have been obtained with the foregoing model, are shown in Figs. 9-10 [34].

4. FRACTURED CONCRETE

4.1 Frictional Limit States

The most important characteristics of the surface cracks in concrete are their surface roughness and the interlocking of the pieces of aggregate which accompanies every tangential relative displacement across the crack. It has been customary in finite element analysis to treat aggregate interlock by considering a nonzero shear stiffness of cracked concrete in the direction parallel to the crack, with a value between 0 and its full elastic value. However, this treatment is incomplete and in some situations certainly inadequate. What is important is that any shear stress transmitted across the crack must be accompanied by significant normal compressive stress on the crack. This stress may produce significant tensile stresses in the reinforcement. The simplest way to treat this phenomenon is to consider it as friction, characterized by certain friction coefficient k (typical value 1.4 to 1.7).

A relatively simple and fundamental problem is that of limit states of a concrete panel intersected by parallel cracks and reinforced in arbitrary directions (Fig. 11). This problem has recently been analyzed taking friction into account [53, 68]. This leads to the following limit state envelope (yield criterion)

$$\left[\left(N_x^s - N_x\right) - \beta_1\left(N_y^s - N_y\right)\right]\left[\left(N_y^s - N_y\right) - \beta_1\left(N_x^s - N_x\right)\right] = \left(2\beta_2 N_{xy}\right)^2 \tag{31}$$

(Fig. 12 and 13) in which

$$\beta_1 = \left[\tan\left(\frac{\pi}{4} - \frac{\beta}{2}\right)\right]^2, \qquad \beta_2 = \left[2\cos\left(\frac{\pi}{4} - \frac{\beta}{2}\right)\right]^{-2} \tag{32}$$

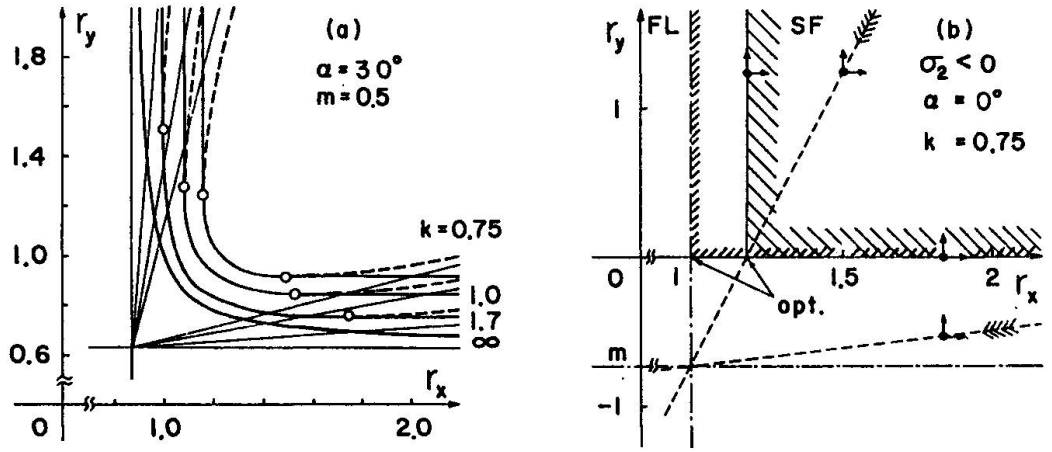

Fig. 12 Example Safe Domain Envelopes of Reinforcement for Given Load for Various Friction Coefficients k after [54,68](r_x, r_y = reinforcement ratios)

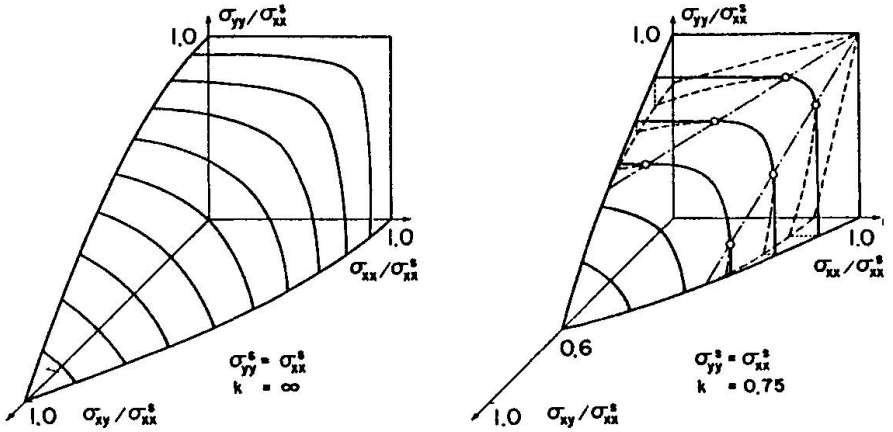

Fig. 13 Example of Yield Surfaces of Net-Reinforced Panel [54,68]

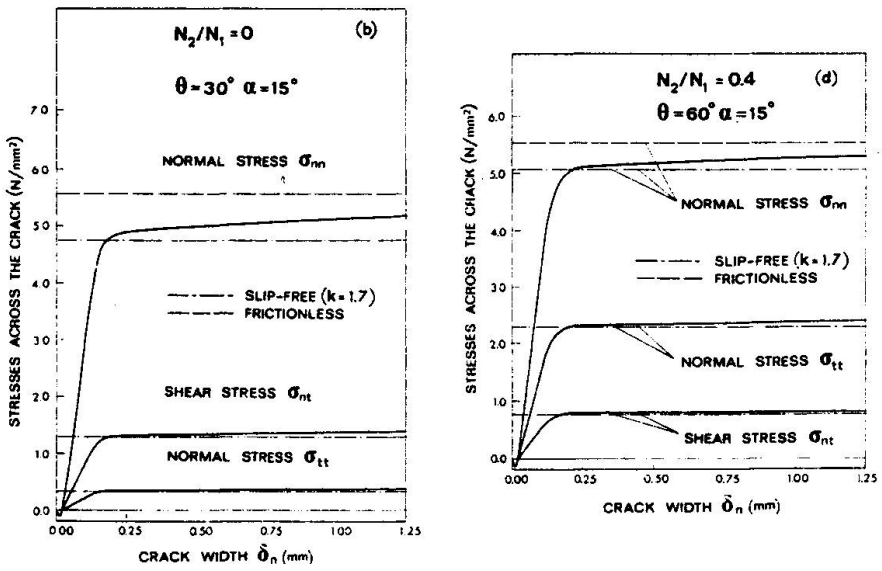

Fig. 14 Predictions of Experimentally Calibrated Rough Crack Model for Stress vs Crack Width Curves of a Reinforced Panel [67]

where β = friction angle on the cracks; N_x^s, N_y^s = required yield forces in the reinforcement in the orthogonal x and y directions; N_x, N_y, N_{xy} = components of the applied internal forces with regard to reinforcement directions. The classical frictionless solution [55,56] represents a special case of this equation for $\beta = \beta_1 = \beta_2 = 0$. The solution of frictional and frictionless yield envelopes and the corresponding yield surfaces are exhibited for a certain loading situation in Figs. 12-13. It is interesting to observe that the frictional design leads to a heavier reinforcement than does the frictionless design, which is obtained as a special case when the friction coefficient approaches infinity, in which case the normal stress corresponding to a shear stress on the crack is zero. The differences due to friction are insignificant when the prinicple directions of applied forces are close to reinforcement directions but they become rather significant when the reinforcement direction significantly deviates from the principle direction of applied forces. Thus, we see that the often stated assumption that the neglect of friction is on the safe side is not true.

The basic assumption which is considered in the limit design of reinforcement is that equilibrium with consideration of friction must be achieved for any direction of cracks in concrete. This assumption differs from that used in plasticity analysis of reinforced concrete in which no crack direction is assumed a priori and is determined from the limit state condition itself. From this fact it may be shown that the frictional limit design with crack of arbitrary direction also never yields less reinforcement than the plasticity analysis (see discussion to Ref. 53).

The frictional limit design with cracks of arbitrary directions has also been carried out for reinforced plates subject to bending and membrane forces. The resulting limit state envelopes again, in general, require more reinforcement than those obtained with the neglect of friction [58].

It must be, however, emphasized that the classical frictionless design approach leads to reinforcement that is safe in the sense of providing equilibrium for a given load. However, the frictionless limit state can be developed only after a very large deformation in which large crack opening is achieved (over 1 cm). This conclusion has been made on the basis of a much more realistic analysis utilizing the experimental stress-displacement relation for cracks [67].

4.2 Deformation Due to Rough Cracks

For the analysis of stresses and strains under given loads, one needs the relationship between the increments of normal and tangential stresses on the crack, σ_{nn} and σ_{nt}, and the relative normal and tangential displacements across the crack, δ_n and δ_t. This relationship may be considered in the form:

$$\begin{Bmatrix} d\sigma_{nn} \\ d\sigma_{nt} \end{Bmatrix} = \begin{bmatrix} B_{nn} & B_{nt} \\ B_{tn} & B_{tt} \end{bmatrix} \begin{Bmatrix} d\delta_n \\ d\delta_t \end{Bmatrix} \tag{33}$$

in which B_{nn}, B_{nt}, ... are the stiffness coefficients of the crack. In the simplest approximation one may base this relationship on the concept of frictional slip with dilatancy, characterized by friction coefficient k and dilatancy ratio α_d defining the ratio of normal to tangential displacements. If k and α_d are considered constant, one may deduce the following incremental stiffness matrix for cracked concrete:

$$\begin{Bmatrix} d\sigma_n \\ d\sigma_t \\ d\sigma_{nt} \end{Bmatrix} = \begin{bmatrix} 1 & \nu & \pm 2\alpha_d \\ \nu & \frac{E_c}{E^*}+\nu^2 & \pm 2\alpha_d \nu \\ \pm k & \pm k\nu & (\pm 2\alpha_d)(\pm k) \end{bmatrix} \begin{Bmatrix} d\epsilon_n \\ d\epsilon_t \\ d\gamma_{nt} \end{Bmatrix} \tag{34}$$

in which the ± signs refer to slips of various directions [54]. An interesting aspect of this stiffness matrix is that it is singular, which is the consequence of the friction relation. However, the singularity of this matrix is not a problem in reinforced concrete because the deformation is stabilized by the reinforcement. The stiffness matrix in Eq. 34 has been used also in the analysis of reinforcing nets and again it was found that in general it requires heavier reinforcement than the classical service stress design with frictionless cracks in the principal strain direction [57].

Experimental evidence [59-65], however, reveals that the crack stiffness coefficients are extremely variable depending on the normal and tangential displacements across the crack. For very small openings, the cracks offer a very large resistance to shear displacement while for large crack openings this resistance may become very small. At small crack openings, even a very small tangential displacement across the crack results in very large compressive stresses, while for large crack openings even large tangential displacements do not produce large compression stresses. Algebraic formulas which describe the dependence of stiffness coefficients B_{nn}, B_{nt}, etc. as determined from test results available in the literature were given in Ref. 67. Superimposing the deformations on the cracks to those due to solid concrete between the cracks, one can obtain the flexibility matrix of cracked concrete. For small crack openings this matrix can be written in an explicit form, as follows [67]:

$$\begin{Bmatrix} d\epsilon_n \\ d\epsilon_t \\ d\gamma_{nt} \end{Bmatrix} = \begin{bmatrix} D_{11}+A|\sigma_{nt}|^p\sigma_{nn}^{-2}, & D_{12}, & \pm A\,p\,|\sigma_{nt}|\sigma_{nn}^{-1} \\ D_{21}, & D_{22}, & 0 \\ \pm B|\sigma_{nt}|^{p+1}\sigma_{nn}^{-2}, & 0, & D_{33}+B(p+1)|\sigma_{nt}|\sigma_{nn}^{-1} \end{bmatrix} \begin{Bmatrix} d\sigma_n \\ d\sigma_t \\ d\sigma_{nt} \end{Bmatrix} \tag{35}$$

in which A, B, p = material constants which depend on crack spacing s, and D_{11}, D_{12} ... = flexibility coefficients of solid concrete between the cracks. The ± sign refers to various directions of shear strain. It is instructive to observe that this matrix contains large off-diagonal terms which determine the normal stress produced by shear strain and the change in shear stress associated with normal strain. Shear stiffness reduction [66] is insufficient [67,54].

For the structural analyst, a natural question is the magnitude of error caused by leaving out the off-diagonal terms or considering them equal to ensure symmetry of the matrix. As explained at the outset, the asymmetry of the stiffness matrix, since it is of frictional type, is not likely to cause instabilities; however, it is inconvenient since most available finite element codes assume symmetric stiffness matrices. This question requires deeper examination but at this time we can say that there exists cases where for which the neglect of the off-diagonal terms is significant. There may of course exist

numerous other cases where it is not so.

As already mentioned, the rough crack model with crack stiffness coefficients determined directly from measurements can be used to predict the limit states. The results of such calculations [67] are exemplified in Fig. 14.

Consideration of crack friction and dilatancy is likely to be most important in dynamic problems, which are normally characterized by highly non-proportional stress histories. Such stress histories in individual finite elements were, for example, observed in large scale dynamic finite element analysis of nuclear prestressed concrete pressure vessels subjected to internal explosive energy release. Fig. 15 shows an example of calculation results from Ref. 69 (these calculations did not include crack friction and dilatancy). The fact that the finite elements undergo cracking in multiple directions is an obvious signal of highly non-proportional stress histories.

5. FRACTURE PROPAGATION

Structural analysis of reinforced concrete necessitates not only the knowledge of the behavior of existing cracks but also of their propagation. For this purpose, it seems preferable to model this phenomenon in terms of element-wide blunt smeared crack band rather than a single sharp interelement crack. This corresponds to the observed fact that cracks in concrete tend to be diffuse and spread over a large zone, especially at the front of propagation. At the same time, the concept of an element-wide blunt smeared crack band is much more convenient than interelement sharp cracks, particularly when the fracture propagates in an unknown and arbitrary direction, proceeding in a skew path through the mesh. Compared to the use of sharp interelement cracks, it is not necessary to split each node in two when the crack advances, and this avoids the need for node renumbering and changes in topological connectivity of the mesh with the necessary recalculations of the structural stiffness matrix. Moreover, when the crack direction is unknown it is not necessary to vary the direction of the interface between two finite elements and move the location of the node into which the crack is about to advance. It suffices to modify the stiffness of the matrix of the finite elements that undergo cracking, setting the normal stiffness in the direction across the cracks equal to zero.

The propagation of smeared crack bands in finite element meshes has so far been determined on the basis of the stress value compared to the strength limit [70, 73]. It has, however, been demonstrated that this approach can give widely different results depending on the choice of the finite element mesh, and is, therefore, unobjective [74-77]. As the size of the finite elements in the region of the crack front is reduced to zero, the crack band tends to localize into a single element strip, and since the stress in the stress in the element in front of the crack band tends to infinity, the load which causes further extension of the crack band is always found to approach zero when the mesh refinement is considered.

5.1 Energy Criterion for Crack Band Propagation

A propagation criterion that is independent of the mesh size is the rate of the energy release per unit length (or in three-dimensions, unit area) of the crack band. This is the same concept as in fracture mechanics of sharp cracks [78]. In a finite element scheme, the energy release rate, G, may be approximated as $\Delta U/\Delta a$, where ΔU is the energy release of the structure as the crack band advances the length Δa of a single finite element. If the value of $G = -\Delta U/\Delta a$ is less

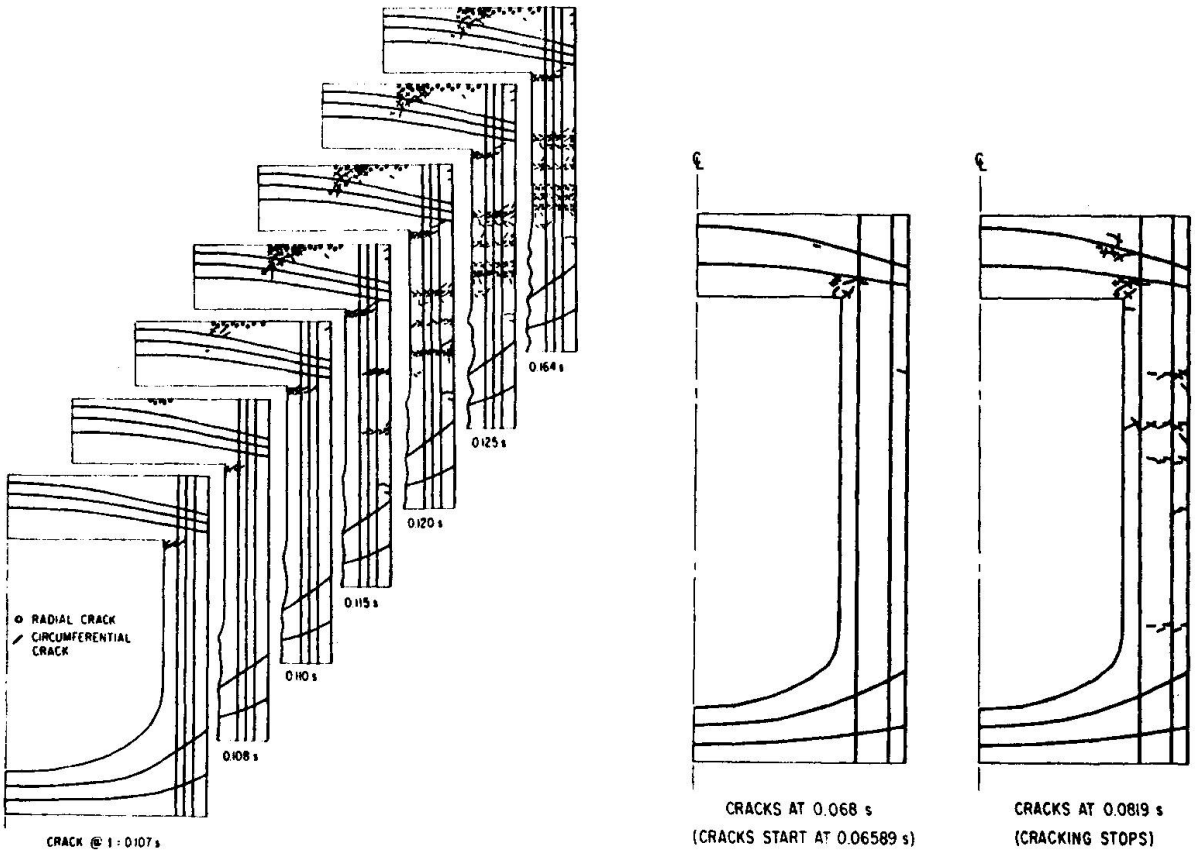

Fig. 15 Example of Cracking Sequence in Dynamic Loading of Concrete Reactor Vessel, Calculated by Finite Elements [69] (Left: Pool-Type vessel, Right: Loop-Type Vessel for LMFBR)

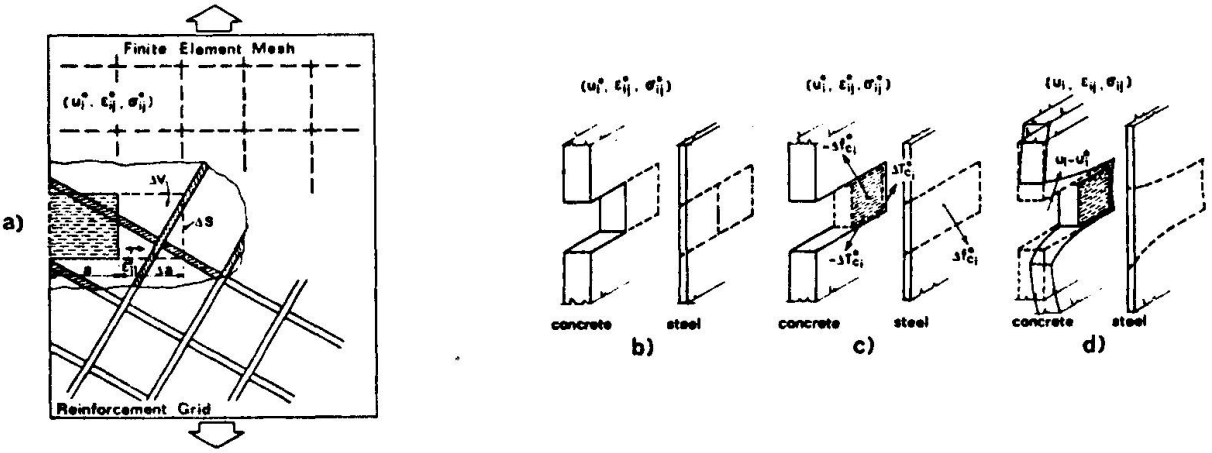

Fig. 16 Crack Band Advance in Finite Element Mesh

than a certain critical energy release rate, G_{cr}, the crack band cannot propagate. If G attains the critical value G_{cr}, the crack band is extended into the next finite element.

The calculation of the energy release, ΔU, may be carried out similarly to Rice's formula for the extension of the notch in an elastic material [78]. The only generalization necessary is to take into account the fact that, in contrast to a notch extension, the material is not removed but merely penetrated by parallel cracks, causing that only part of the energy stored in the material is lost by the crack band extension [75]. A second generalization necessary for reinforced concrete is to take into account the effect of reinforcing bars crossing the finite element into which the cracks propagate [76].

The change of the potential energy of an elastic body due to the extension of the crack band into a volume ΔV of the element in front of the crack band is independent from the history in which this extension happens and may, therefore, be separated into two stages:

Stage I. - Volume ΔV of the element ahead of the crack band gets intersected by cracks in the direction of the principal tensile stress (Fig. 16). At the same time, the stress and deformation state in the rest of the body is imagined to remain fixed (frozen). Accordingly, one must introduce surface tractions ΔT^{o}_{ci} acting on the boundary ΔS of volume ΔV, and in case of reinforced concrete, also forces Δf^{o}_{ci} transmitted from steel into concrete within volume ΔV. These tractions and forces are calculated so as to replace the previous action of the volume ΔV of the concrete upon the rest of the body (Fig. 16c).

Stage II. - Forces ΔT^{o}_{ci} and Δf^{o}_{ci} are then released by gradually applying the opposite forces $-\Delta T^{o}_{ci}$ and $-\Delta f^{o}_{ci}$ (Fig. 16).

The energy changes corresponding to these two stages may be expressed as

$$\Delta W_{(\Delta V)} = -\int_{\Delta V} \frac{1}{2}\left(\sigma^{c^{o}}_{ij}\varepsilon^{o}_{ij} - E'_{c}\varepsilon^{o^{2}}_{11}\right) dV \tag{36}$$

$$\Delta L = \int_{\Delta S} \frac{1}{2}\,\Delta T^{o}_{c_i}\left(u_i - u^{o}_{i}\right) dS + \int_{\Delta V} \frac{1}{2}\,\Delta f^{o}_{c_i}\left(u_i - u^{o}_{i}\right) dV \tag{37}$$

and the total energy release associated with the single element advance of the crack band is

$$\Delta U = \Delta W_{(\Delta V)} + \Delta L \tag{38}$$

Here, u_i = displacements in cartesian coordinates x_i $(i = 1,2,3)$, σ_{ij} = cartesian stress components, ε_{ij} = cartesian components of the small strain tensor, superscript c refers to concrete, u^{o}_{i}, ε^{o}_{ij}, and $\sigma^{c^{o}}_{ij}$ = values of displacements, strains and stresses in volume ΔV before the advance of the crack band (before Stage I); $E'_c = E_c$ for plain stress and $E'_c = E_c/(1-\nu_c^2)$ for plain strain, in which E_c = Young's modulus for plain concrete and ν_c = Poisson's ratio.

The foregoing equations constitute the basic energy relations for the propagation of crack bands in reinforced concrete. These equations apply only for linearly elastic behavior outside the crack band. It is, however, possible

[76] to generalize the expression for ΔU for the case of nonlinear behavior of concrete outside the crack band and for the yielding of steel. To this end, the coefficients 1/2 in the expression for ΔU must be replaced by integrations over the deformation path of Stage II. In case of nonlinear behavior an additional restriction must be imposed; namely, the width w of the element-wide crack band either must coincide with the actual crack band width w_c for the material or one must use a path-independent integral such as the J integral instead of Eq. 37. This is necessary because the nonlinear behavior also causes a loss of energy which must be distinguished from the loss of energy due to fracture extension.

5.2 Effect of Bond-Slip of Reinforcement

In finite element analysis of reinforced concrete it has been customary to assume that the steel bars are rigidly attached to concrete at the nodes. This treatment is, however, not only physically unjustified but also unobjective and leads to incorrect convergence. The bars connecting the nodes on the opposite sides of the crack band represent an elastic connection, the stiffness of which is inversely proportional to the distance between the nodes, i.e., to the width w of the crack band. Thus, as the width of the crack band tends to zero, the stiffness of the connection across the crack band increases to infinity, which in the limit prevents any opening of the crack band. So it is clear that no cracking can be obtained in the limit. Moreover, one can check that significant differences of the results are caused by the lack of bond-slip than when meshes of various practically possible sizes are considered [75-77].

To obtain an objective and properly convergent formulation, one must take into account the bond-slip. The bond-slip in reality occurs over a certain length, L_s (Fig. 17). The most realistic treatment of the bond-slip would call for using separate nodes for concrete and steel connected by some nonlinear linkage elements representing forces transmitted by bond. However, this approach would be quite cumbersome. In the spirit of the approximations involved in the smeared crack band model, it should be sufficient to introduce the bond slip in such a way that the stiffness of the connection provided by the steel bars crossing the crack band would be roughly correct and independent of the mesh size.

So, for the sake of simplicity, the actual curvilinear variation of the bond forces and the axial forces in the bars (Fig. 17) may be replaced by an idealized piece-wise variation of the bond force and the corresponding piece-wise linear variation of the actual axial force in the bars. The latter may further be replaced by a piece-wise constant variation of the axial force, such that the overall extension of the bar over the distance of the bond-slip be roughly the same. The actual distance of the bond slip may be approximated as

$$L_s = \frac{(\sigma_s - \sigma_s')A_b}{U_b'} \tag{39}$$

in which A_b = cross-sectional area of the steel bar; σ_s = tensile stress in the bar at the point it crosses the crack band; σ_s' = tensile stress in the bar at the end of the slipping segment, i.e., at locations sufficiently remote from the crack band; and U_b' = the ultimate bond force as determined from pull-out tests. Certain reasonable estimates of σ_s and σ_s' can be made on the basis of the yield stress of steel and the tensile strengths of concrete [76].

Expression (39) gives the actual bond-slip length as a fixed property characteristic of the steel-concrete composite. For the purpose of finite element analysis, the actual bond-slip length L_s may be replaced by some modified length L_s^* (Fig. 17f) such that the steel stress over this length is uniform and the slip of steel bar within concrete may be considered as free. The length L_s^* is determined from the condition that the extension of the steel bar over the length L_s be the same, as already stated. In this manner, the following expression for the equivalent free bond-slip length can be obtained [72]:

$$L_s^* = \frac{L_s}{2} \frac{p^*}{p(1 + pn - p^*n)} + k_b \frac{w}{2} \tag{40}$$

Here w represents the width of the element-wide crack band, k_b is a correction factor smaller than 1.0 but close to 1.0 (for which also a theoretical expression exists)[72], p is the reinforcement ratio (the ratio of the cross-section areas of reinforcement and concrete), n is the ratio of Young's modulus of steel to that of concrete, and p^* is a certain modified reinforcement ratio which may be conveniently chosen so as to make the length L_s^* equal to the distance between the adjacent nodes located across the crack band (L_s' in Fig. 17h).

5.3 Typical Numerical Results

Some typical numerical finite element results [76] are plotted in Fig. 17. Considered is a rectangular reinforced concrete panel subjected to tensile forces at two opposite ends. A symmetric centrally located crack band normal to the applied loads is assumed to grow from the center of the panel symmetrically towards its sides. Using the energy criterion and the free bond-slip length, one can calculate the multiplier α of the applied loads that is necessary to cause the extension of the crack band of length a; see [76]. As expected, multiplier α decreases as the crack band length a increases. Computations have been carried out [76] for three different rectangular meshes, the sides of which are in the ratio 4:2:1, labeled as A, B, C (Fig. 17 i). The grid used in the calculations was a uniform square grid and each square element was assumed to consist of two constant strain triangles. Both triangular elements forming one square were assumed to always crack simultaneously.

It may now be observed in Fig. 17 i that the results for the three different meshes fall approximately on the same curve. It has been previously demonstrated [75] that in case of the classical strength criterion, the results of the calculation for these three meshes are widely different and deviate from each other as much as 100%. It is also noteworthy that coincidence of the results is obtained for plain concrete ($p = 0$) as well as for reinforced concrete($p > 0$). It has been also previously shown [72] that the results for reinforced concrete for these three meshes are far apart when the strength criterion is used, and also when the energy criterion without the bond slip of steel is considered.

The results presented in Fig. 17 i and numerous further results given in [75,76] demonstrate that the proposed method is objective, i.e., independent of the chosen finite element mesh.

The solid curves indicated in Fig. 17 i represent the exact solutions for a sharp crack according to linear fracture mechanics. From this comparison it is seen that the concept of an element-wide crack band may be also used as a convenient and effective approximation to the propagation of sharp cracks, gaining all the practical computational advantages of the blunt smeared crack band model as compared to considering sharp inter-element cracks. One may now naturally

ask: What is then the physical difference between the smeared crack band and the sharp inter-element crack?

Obviously, up to a certain rather wide crack band the difference is insignificant in these computations. For finer meshes, the real difference arises only through the value of the energy-release rate that is to be considered in the calculation. In an on-going work that has not yet been completed, it is found that the critical energy release rate for a smeared crack band cannot be considered to be a fixed material property (unless the width of the band tends to zero), and must be regarded as a function of the band width as well as of the rate of change of G and of the stiffness of the structure surrounding the front of the crack band. When the differences in the critical energy release rate between a smeared crack band and a sharp crack are considered, the results of computations cannot be, of course, identical. It is by means of the variation of the critical energy release rate that one can explain deviations from fracture mechanics predictions as observed on concrete specimens the size of which is not sufficiently large compared to the aggregate size [82,79-81].

5.4 Equivalent Strength Criterion

Determination of the energy release ΔU needed for the propagation criterion requires two finite element calculations, one for the initial crack band length and one for the crack band extended by one element. It has been found [75,76] that calculations may be simplified by approximately estimating the energy release rate on the basis of the stress state in the uncracked finite element just in front of the crack band. The energy release rate becomes (approximately) critical when the normal stress orthogonal to the crack direction attains the value

$$(\sigma^{o}_{22})_{cr} = \sigma_{eq} = c\sqrt{\frac{E'_c\, G_{cr}}{w}} \tag{41}$$

in which σ_{eq} was named the equivalent strength, and c is a coefficient characteristic of the given element type. Generally, c is close to 1.0. For a square element consisting of four linear strain triangles, $c = 0.826$ [77] while for a square element consisting of only two constant strain triangles $c = 0.921$ [75,76]. It is interesting to observe that σ_{eq} increases as the width of the crack band decreases, and tends to infinity as the element size approaches zero. Obviously, the equivalent strength criterion in Eq. (41) must give results that significantly differ from those for a constant strength limit. In a work still in progress, it has been found that the equivalent strength criterion, which is in Eq. (41) given only for plain concrete, may be extended to reinforced concrete. For this purpose, a corrective term which involves a reinforcement ratio must be added to the expression in Eq. 41.

5.5 Basic Results

The research results just outlined lead to several important conclusions: (1) The use of a constant strength limit for determining extension of a crack band in a finite element mesh is unobjective and has incorrect convergence behavior. The results may differ by as much as 100% when meshes of different size are used. (2) An objective and physically realistic criterion for crack band extension must be expressed in terms of the energy release rate by unit length of the crack band. Expressions for calculating the energy release rate in a finite element program have been formulated. (3) To achieve an objective and properly convergent propagation criterion for reinforced concrete, the bond-slip between steel reinforcement and concrete must be taken into account. This may be conveniently done in terms of the equivalent free bond-slip length, for which a

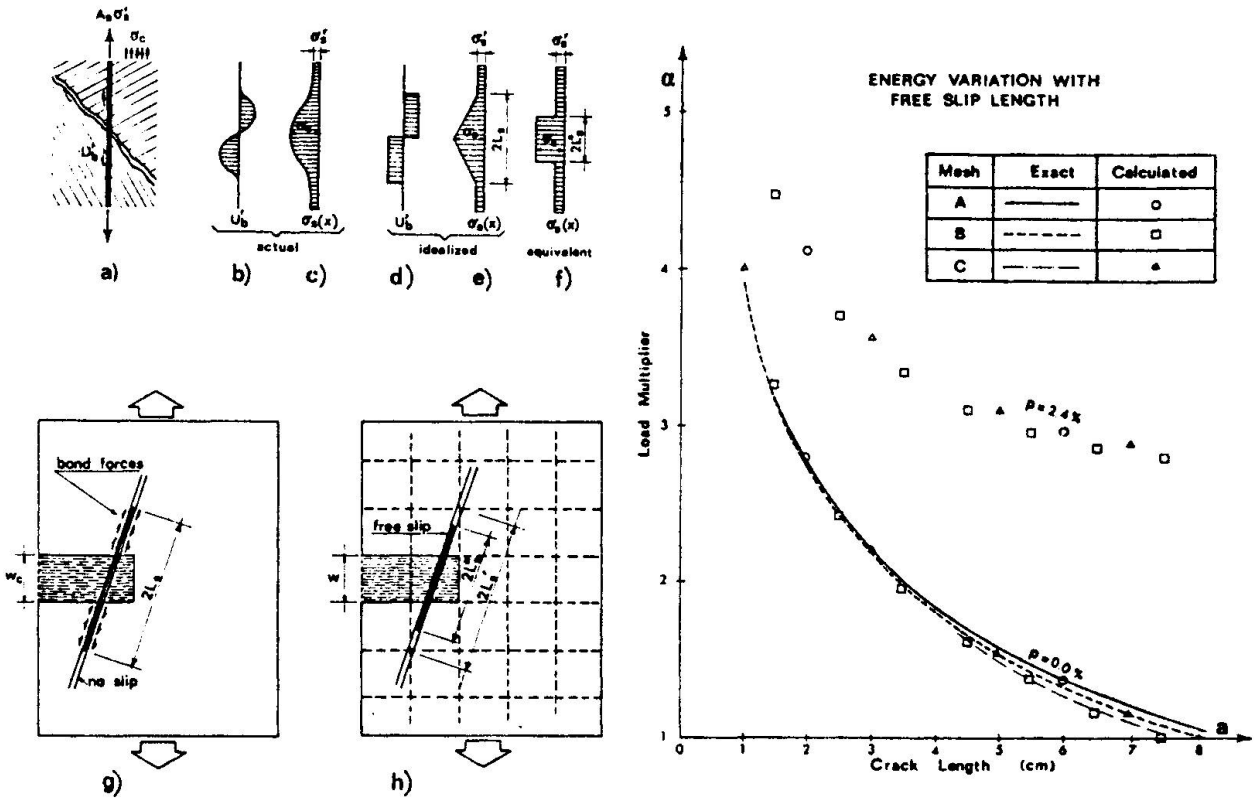

Fig. 17 Effect of Bond Slip and Some Typical Numerical Results [76]

simple approximation exists. (4) As an acceptable approximation, the energy criterion may be replaced by an equivalent strength criterion such that the strength limit depends on the width of the element-wise smeared crack band.

6. CONCLUDING REMARKS

One major impression which may result from this exposition is that the advanced theories of the mechanical behavior of concrete are not, in the most part, very simple. This fact is certainly unappealing to a structural analyst, and it would be outright objectionable to a physicist who knows that the true form of the laws of nature is simple, not complicated. We must recognize, however, that we don't move here in the world of a physicist whose mind is occupied only with the fundamental laws describing individual physical phenomena. The response of heterogeneous composite such as concrete is influenced by numerous physical phenomena and processes intervening simultaneously. Realizing this, it should not be altogether surprising to us that we have been unable so far to describe the complicated response of concrete by a few simple laws. We must certainly strive hard for such an outcome, but at best we probably achieve it only to a limited extent. Fortunately, we are blessed with powerful tools, the electronic computers, which can handle even rather complicated mathematical models. It is due to this fortunate situation that our effort to develop more accurate, realistic and refined mathematical models of concrete should bear fruit.

7. ACKNOWLEDGMENT

Support by the U.S. National Science Foundation under Grant ENG75-14848-A01 to Northwestern University is gratefully acknowledged. Thanks are also due to Theresa Flanagan who perfectly transcribed this paper from an imperfect tape-recorded dictation, filtering out the sounds of waves, wind, children and the like.

8. REFERENCES

1. Drucker, D.C., "Some Implications of Work Hardening and Ideal Plasticity," Quarterly of Applied Math., Vol. 7, 1950, pp. 411-418.

2. Drucker, D.C., "A Definition of Stable Inelastic Material," J. Appl. Mech., Trans. ASME, Vol. 26, 1959, pp. 101-106.

3. Fung, Y.C., "Foundations of Solid Mechanics," Prentice Hall, Englewood Cliffs, N.J., 1975 (Chapter 6).

4. Malvern, L.E., "Introduction to the Mechanics of a Continuous Medium," Prentice-Hall, Englewood Cliffs, N.J., 1969.

5. Bažant, Z.P., "Work Inequalities for Plastic-Fracturing Materials," Intern. J. of Solids and Structures, Vol. 16, 1980.

6. Bažant, Z.P., Kim, S.S., "Plastic-Fracturing Theory for Concrete," J. of the Engng. Mech. Div., Proc. Am. Soc. of Civil. Engrs., Vol. 105, June 1979, pp. 407-428, with Errata in Vol. 106 (also as Preprint 3431, ASCE Annual Convention, Chicago, Oct. 1978).

7. Schapery, R.A., "On a Thermodynamic Constitutive Theory and Its Applications to Various Nonlinear Materials," Proc. IUTAM Symp. East Kilbride, June 1968, ed. B.A. Boley, Springer Verlag, New York, 1968.

8. Valanis, K.C., "A Theory of Viscoplasticity without a Yield Surface," Archiwum Mechaniki Stossowanej (Archives of Mechanics, Warsaw), Vol. 23, 1971, pp. 517-551.

9. Bažant, Z.P., Bhat, P., "Endochronic Theory of Inelasticity and Failure of Concrete," J. of the Engrg. Mech. Div., Proc. Am. Soc. of Civil Engrs., Vol. 102, 1976, pp. 701-722.

10. Bažant, Z.P., Shieh, C.L., "Total Strain Theory and Path-Dependence of Concrete," J. of the Engng. Mech. Div., Proc. ASCE, Vol. 106, Oct. 1980 pp.

11. Sørensen, S.I., Arnesen, A., Bergan, P.G., "Nonlinear Finite Element Analysis of Reinforced Concrete Using Endochronic Theory," Finite Elements in Nonlinear Mechanics (Proc. of Int. Conf. held at Geilo, Norway, 1977) Tapir, Norwegian Inst. of Tech. Trondheim, Vol. 1, pp. 167-190, 1978.

12. de Villiers, I.P., "Implementation of Endochronic Theory for Analysis of Concrete Structure," Ph.D. Dissertation, University of California,Berkeley 1977.

13. Dougill, J.W., "On Stable Progressively Fracturing Solids," ZAMP (Zeitschrift für Angewandte Mathematik und Physik), Vol. 27, Fasc. 4, 1976, pp. 423-437.

14. Dougill, J.W., "Some Remarks on Path Independence in the Small in Plasticity," Quarterly of Appl. Math., Vol. 32, 1975, pp. 233-243.

15. Mandel, J.,"Conditions de Stabilité et Postulat de Drucker," in Rheology and Soil Mechanics," IUTAM Symp. held in Grenoble in 1964, ed. by J. Kravtchenko and P.M. Sirieys, Springer Verlag, Berlin, 1966, pp. 58-68.

16. Maier G., "Incremental Plastic Analysis in the Presence of Large Displacements and Physical Stabilizing Effects," Int. J. of Solids and Structures, Vol. 1, 1971, pp. 345-372.

17. Bažant, Z.P., "Instability, Ductility and Size Effect in Strain-Softening Concrete", J. of the Engineering Mechanics Division, Proc. ASCE, Vol. 102, April 1976, EM2, pp. 331-344.

18. Hill, R., Rice, J.R., "Elastic Potentials and the Structure of Inelastic Constitutive Laws," SIAM J. of Appl. Math., Vol. 25, No. 3, 1973 pp. 448-461.

19. Sandler, I.S., "On the Uniqueness and Stability of Endochronic Theories of Material Behavior," Trans. ASME, Series E, Journal of Applied Mechanics, Vol. 45, 1978, pp. 263-266.

20. Rivlin, R.S., "Some Comments on the Endochronic Theory of Plasticity," Report No. CAM-100-33, Center for the Application of Math., Lehigh Univ., Bethlehem, 1979; to appear in Int. J. of Solids and Structures.

21. Bažant, Z.P., "Endochronic Inelasticity and Incremental Plasticity," Int. J. of Solids and Structures, Vol. 14, 1978, pp. 691-714.

22. Bažant, Z.P., Bhat, P., "Endochronic Theory of Inelasticity and Failure of Concrete," J. of the Engrg Mech. Div., ASCE, Vol. 102, No. EM4, Proc. Paper 12360, April 1976, pp. 701-722.

23. Aschl, H., Linse, D., Stoeckl, S., "Strength and Stress-Strain Behavior of Concrete under Multiaxial Compression and Tension Loading," Technical Report, Technical University, Munich, Germany, Aug. 1976.

24. Balmer, G.G., "Shearing Strength of Concrete under High Triaxial Stress-Computation of Mohr's Envelope as a Curve," Structural Research Laboratory Report No. SP-23, Structural Research Laboratory, Denver, Colo. Oct. 1949.

25. Bresler, B., Pister, K.S., "Strength of Concrete under Combined Stresses," American Concrete Inst. Journal, Vol. 551, Sept. 1958, pp. 321-345.

26. Budiansky, B., O'Connell, R.J., "Elastic Moduli of Cracked Solids," Int. J. of Solids and Structures, Vol. 12, 1976, pp. 81-97.

27. Drucker, D.C. and Prager, W., "Soil Mechanics and Plastic Analysis or Limit Design," Quarterly of Appl. Math., Vol. 10, 1952, pp. 157-165.

28. Hobbs, D.W., "Strength and Deformation Properties of Plain Concrete Subject to Combined Stresses, Part 3: Results Obtained on a Range of Flint Gravel Aggregate Concrete," Technical Report, Cement and Concrete Association, London, England, July 1974.

29. Kupfer, H.B., Hilsdorf, H.K., Rüsch, H., "Behavior of Concrete under Biaxial Stresses," American Concrete Inst. Journal, Vol. 66, 1969, pp. 656-666.

30. Liu, T.C.Y., Nilson, A.H. and Slate, F.O., "Biaxial Stress-Strain Relations for Concrete," J. of the Struct. Div., ASCE, Vol. 98, No. ST5, Proc. paper 8905, May, 1972, pp. 1025-1034.

31. Popovics, S., "A Numerical Approach to the Complete Stress-Strain Curves of Concrete," Cement and Concrete Research, Vol. 3, No. 5, Sept. 1973, pp. 583-599.

32. Shah, S.P., Chandra, S., "Critical Stress, Volume Change and Microcracking of Concrete," American Concrete Inst. Journal, Vol. 65, No. 9, Sept. 1968, pp. 770-781.

33 Bažant, Z.P., Panula, L., "Statistical Stability Effects in Concrete Strength and Ductility," J. of the Engng. Mech. Div. Proc., ASCE, Vol. 104, 1978, pp. 1195-1212.

34. Bažant, Z.P., Oh, Byung H., "Strain-Rate Effect in Rapid Nonlinear Triaxial Deformation of Concrete," Structural Engineering Report No. 80-7/640s, Northwestern University, July 1980.

35. Abrams, D.A., "Effect of Rate of Application of Load on the Compressive Strength of Concrete," Proc. ASTM, Volume 17, Part II, pp. 364.

36. Atchley, B.L., Furr, H.L., "Strength and Energy Absorption Capabilities of Plain Concrete Under Dynamic and Static Loadings," American Concrete Inst. Journal, Volume 64, No. 11, Nov. 1967, pp. 745-756.

37. Bresler, B., Bertero, V.V., "Influence of High Strain Rate and Cyclic Loading on Behavior of Unconfined and Confined Concrete in Compression," Report, Division of Structural Engineering and Structural Mechanics, University of California, Berkeley, California, 1979.

38. Dilger, W.H., Kock, R., and Kowalczyk, R., "Ductility of Plain and Confined Concrete under Different Strain Rates," presented at ACI Meeting, Houston, Nov. 1978, ACI Special Publication - to appear.

39. Hatano, T., Tsutsumi, H., "Dynamic Compressive Deformation and Failure of Concrete under Earthquake Load," Proc. of the 2nd World Conference on Earthquake Engineering, Science Council of Japan, Tokyo, 1960. Volume IV, pp. 1963-1978.

40. Mainstron, R.J., "Properties of Materials at High Rates of Straining or Loading," Materials and Structures, Volume 8, No. 44, pp. 108-116.

41. McHenry, D, Shideler, J.J., "Review of Data on Effect of Speed in Mechanical Testing of Concrete," ASTM Special Technical Publication No. 185, pp. 72-82.

42. Rasch, C., "Stress-Strain Curves of Concrete and Stress Distribution in the Flexural Compression Zone under Constant Strain Rate," (in German), Duetscher Ausschuss Für Stahlbeton, Bulletin No. 154, Berlin, 1962.

43. Watstein, D, "Effect of Straining Rate on the Compressive Strength and Elastic Properties of Concrete," American Concrete Inst. Journal, Vol. 49, No. 8, April 1953, pp. 729-744.

44. Watstein, D., "Properties of Concrete at High Speek of Loading," Symposium on Impact Testing, STP No. 176, ASTM, 1956, pp. 150-169.

45. Bažant, Z.P., Asghari, A.A., "Constitutive Law for Nonlinear Creep of Concrete," J. of the Eng. Mech. Div., ASCE, Vol. 103, No. EM1, Proc. Paper 12729, Feb. 1977, pp. 113-124.

46. Bažant, Z.P., Kim, S.-S., "Nonlinear Creep of Concrete-Adaptation and Flow" J. of the Engrg. Mech. Div., ASCE, Vol. 105, No. EM3, Proc. Paper 14654, June 1979, pp. 429-446.

47. Bažant, Z.P., "Theory of Creep and Shrinkage in Concrete Structures: A Précis of Recent Developments," Mechanics Today, Vol. 2, Pergamon Press, Inc., New York, 1975, pp. 1-93.

48. Bažant, Z.P., Osman, E., "Double Power Law for Basic Creep of Concrete," Materials and Structures, Paris, France, Vol. 9, 1976, pp. 3-11.

49. Bažant, Z.P., Panula, L., "Prediction of Time-Dependent Deformations of Concrete," Materials and Structures, Paris, France, Parts I and II, Vol. 11, No. 65, 1978, pp. 307 - 328; Parts III and IV, Vol. 11, No. 66, 1978, pp. 415-434; Parts V and VI, Vol. 12, No. 69, 1979

50. Bažant, Z.P., "Critique of Orthotropic Models and Triaxial Testing of Concrete and Soils," Structural Engineering Report No. 79-10/640c, Northwestern University, Evanston, Illinois, October 1979.

51. Truesdell, C., "Hypo-elasticity," Journal of Rational Mechanics Analysis, Vol. 4, 1955, pp. 83-133.

52. Coon. M.D., Evans, R.J., "Incremental Constitutive Laws and their Associated Failure Criteria with Application to Plain Concrete," Int. J. of Solids and Structures, Vol. 8, 1972, pp. 1169-1180.

53. Bažant, Z.P., Tsubaki, T., "Concrete Reinforcing Net: Optimum Slip-Free Limit Design," J. of the Struct. Div., Proc. ASCE, Vol. 105, 1979, pp. 327-346; Discussion Vol. 106.

54. Bažant, Z.P., Tsubaki, T., "Slip-Dilatancy Model for Cracked Reinforced Concrete," J. of the Struct. Div. Proc., ASCE, Vol. 106, Sept. 1980, pp.

55. Baumann, T., "Zur Frage der Netzbewehrung von Flächentagwerken," Der Bauingenieur, Vol. 47, No. 10, 1972, pp. 367-377.

56. Brondum-Nielsen, T., "Optimum Design of Reinforced Concrete Shells and Slabs," Report No. R.44, Structural Research Laboratory, University of Denmark, Copenhagen, Denmark, 1974, pp. 190-200.

57. Duchon, N.B., Analysis of Reinforced Concrete Membrane Subject to Tension and Shear," American Concrete Inst. Journal, Proc. Vol. 69, No. 9, Sept. 1972, pp. 578-583.

58. Morley, C.T., "Skew Reinforcement of Concrete Slabs against Bending and Torsional Moments," The Institution of Civil Engineers, Proceedings, Vol. 42, Jan. 1969, pp. 57-74.

59. Buyukozturk, O., Leombruni, P., Connor, J., "Analysis of Shear Transfer in Reinforced Concrete with Application to Containment Wall Specimens," Research Report R72-26, Dept. of Civil Engineering, Massachusetts Institute of Technology, Cambridge, Mass, June 1979.

60. Fenwick, R.C., "The Shear Strength of Reinforced Concrete Beams, " thesis presented to the University of Canterbury, at Christchurch, New Zealand, in 1966, in partial fulfillment of the requirements for degree of Doctor of Philosophy.

61. Hofbeck, J.A., Ibrahim, I.O., and Mattock, A.H., "Shear Transfer in Reinforced Concrete," J. of the American Concrete Inst. Vol. 66, No. 13, Feb. 1969, pp. 119-128.

62. Houde, J. Mirza, M.S., "A Finite Element Analysis of Shear Strength of Reinforced Concrete Beams," Special Publication SP42, American Concrete Inst., 1974, pp. 103-128.

63. Paulay, T., Loeber, P.J., "Shear Transfer by Aggregate Interlock," Special Publication SP42, American Concrete Inst., 1974, pp. 1-15.

64. Jimenez-Perez, R., Gergely, P., White, R.N., "Shear Transfer Across Cracks in Reinforced Concrete," Report 78-4, Dept. of Structural Engineering, Cornell University, Ithaca, NY, Aug. 1978.

65. Mattock, A.H., "Shear Transfer in Concrete Having Reinforcement at an Angle to the Shear Plane," Special Publication SP42, American Concrete Inst., 1974, pp. 17-42.

66. Yuzugullu, O., Schnobrich, W.C., "A Numerical Procedure for the Determination of the Behavior of a Shear Wall Frame System," American Concrete Inst. Journal, Vol. 70, No. 7, July 1973, pp. 474-479.

67. Bažant, Z.P., and Gambarova, P.,"Rough Cracks in Reinforced Concrete," J. of the Struct. Div., Proc. ASCE, Vol. 106, 1980, pp. 819-842.

68. Bažant, Z.P., Tsubaki, T., Belytschko, T.B., "Concrete Reinforcing Net: Safe Design," J. of the Struct. Div., Proc. ASCE, Vol. 106, Sept. 1980, pp.

69. Marchertas, A.H., Fistedis, S.H., Bažant, Z.P., and Belytschko, T.B., Analysis and Application of Prestressed Concrete Reactor Vessels for LMFBR Containment, Nuclear Engng. and Design, Vol. 49, July 1978, pp. 155-173.

70. Cedolin, L., and Dei Poli, S., "Finite Element Studies of Shear-Critical R/C Beams," J. of the Engng. Mech. Div. ASCE, Vol. 103, No. 12968, June 1979, pp. 395-410.

71. Ngo, D., Scordelis, A.C., "Finite element Analysis of Reinforced Concrete Beams," J. of the American Concrete Inst., Vol. 66, No. 3, March 1967, pp. 152-153.

72. Scordelis, A.C., "Finite element Analysis of Reinforced Concrete Structures" Proceedings, Specialty Conf. on Finite Element Methods In Civil Engrg., McGill University, Montreal, Quebec, Canada, 1972, pp. 71-113.

73. Suidan, M., and Schnobrich, W.C., "Finite Element Analysis of Reinforced Concrete," J. of the Struct. Div., ASCE, Vol. 99, No. ST10, Proc. Paper 10081, Oct. 1973, pp. 2109-2122.

74. Bažant, Z.P., "Instability, Ductility, and Size Effect in Strain-Softening Concrete," J. of the Engineering Mech. Div., ASCE, Vol. 102, No. EM2, Proc. Paper 12042, April 1976, pp. 331-344.

75. Bažant, Z.P., Cedolin, L., "Blunt Crack Band Propagation in Finite Element Analysis," J. of the Eng. Mech. Div., Proc. ASCE, Vol. 105, No. EM2, April 1979, pp. 297-315.

76. Bažant, Z.P., Cedolin, L., "Fracture Mechanics of Reinforced Concrete," Structural Engng. Report No. 79-9/640m, Dept. of Civil Engineering, Northwestern University, Sept. 1979, to also appear in Journal of the Struct. Div., ASCE.

77. Cedolin, L. and Bažant, Z.P., "Effect of Finite Element Choice in Blunt Crack Band Analysis," Struct. Engineering Report No. 79-6/640e, Dept. of Civil Engineering, Northwestern Univ., June 1979, also Computer Methods in Applied Mechanics and Engineering, 1980, in press.

78. Rice, J.R., "Mathematical Analysis in the Mechanics of Fracture," Fracture, an Advanced Treatise, H. Liebowitz, ed., Vol. 2, Academic Press, New York, 1968, pp. 191-250.

79. Hawkins, N.M., Wyss, A.N. and Mattock, A.H., "Fracture Analysis of Cracking in Concrete Beams," J. of the Struct. Div., ASCE, Vol. 103, No. ST5, Proc. Paper 12921, May, 1977, pp. 1015-1030.

80. Kaplan, M.F., "Crack Propagation and the Fracture of Concrete," American Concrete Inst. Journal, Vol. 58, No. 11, Nov. 1961.

81. Shah, S.P., McGarry, F.J., "Griffith Fracture Criterion and Concrete," J. of the Engrg. Mech. Div., ASCE, Vol. 97, No. EM6, Proc. Paper 8597, Dec. 1971, pp. 1163-1976.

82. Walsh, P.F., "Fracture of Plain Concrete," The Indian Concrete Journal, Vol. 46, No. 1972, pp. 469, 470, and 476.

Leere Seite
Blank page
Page vide

Material Modeling of Reinforced Concrete

Modèle de comportement du béton armé

Modelle für das Stahlbetonverhalten

KURT H. GERSTLE
Professor of Civil Engineering
University of Colorado
Boulder, CO, USA

SUMMARY

This report presents an overview of the current state of knowledge of the behavior of reinforced concrete and its formulation for finite-element analysis. Aspects of material behavior covered include elastic and inelastic response, including yielding of the steel and crushing and cracking of concrete, leading to anisotropic action, force transfer across cracks, and bond deterioration between steel and concrete. The importance of assessing the influence of these different phenomena is pointed out.

RESUME

Ce rapport donne un aperçu de l'état actuel des connaissances sur le comportement du béton armé et sur sa formulation pour l'analyse par la méthode des éléments finis. Les différents aspects du comportement des matériaux comprennent, outre le comportement élastique et inélastique, la plastification de l'acier, la fissuration et l'écrasement du béton; ceci conduit à un effet d'anisotropie, à une transmission d'efforts à travers les fissures et à une diminution de l'adhérence entre acier et béton. Il est important d'estimer correctement les différents phénomènes.

ZUSAMMENFASSUNG

Dieser Bericht gibt einen Überblick über den gegenwärtigen Stand der Kenntnis des Stahlbetons und seiner Formulierung für Berechnungen mit finiten Elementen. Die behandelten Aspekte des Materialverhaltens betreffen elastisches und inelastisches Verhalten einschliesslich Fliessen des Stahls, Rissbildung und Versagen des Betons. Diese Erscheinungen führen zu anisotropem Verhalten, zur Kraftübertragung an Rissen und zur Verschlechterung des Verbunds zwischen Stahl und Beton. Es ist wichtig, die verschiedenen Phänomene richtig einzuschätzen.

1. FINITE-ELEMENT FORMULATION

1.1 General Formulation

Finite-element analysis is based on subdividing the structure into a number of discrete elements, connected to each other at individual joints, as shown in Fig. 1. The nodal displacements $\{\Delta\}$ are determined by the stiffness, or displacement, method, in which the nodal forces $\{X\}$ are related to these displacements by the structure stiffness matrix $[K]$:

$$\{X\} = [K]\{\Delta\} \quad . \tag{1}$$

The matrix $[K]$ contains the material properties; if these can be represented by linear relations, as in elastic analysis, the stiffnesses are constants, and the determination of the unknowns is a straightforward problem of solving a set of linear simultaneous equations. Non-linear material behavior, as in reinforced concrete, is often modelled as piecewise-linear, and solved in a step-by-step fashion.

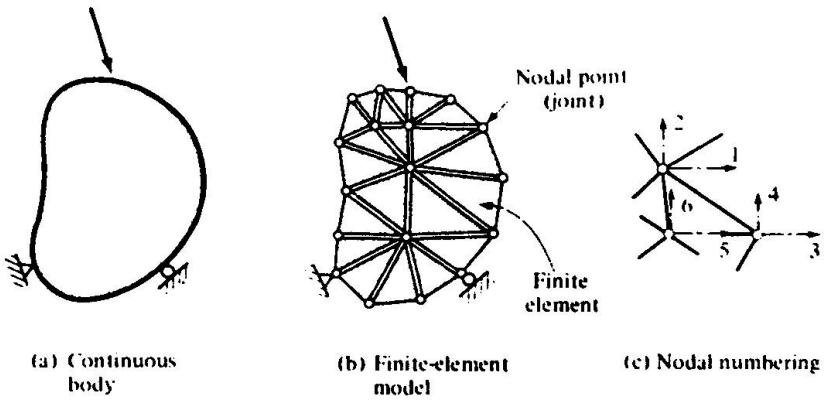

Fig. 1 Finite-element Model

The structure stiffness matrix $[K]$ can be assembled by superposition of the element stiffness matrices $[k]$; equilibrium demands that

$$[K] = \sum_i [k^i] \tag{2}$$

The stiffness matrix $[k^i]$ contains the material properties of Element i, of volume V:

$$[k^i] = \int_V [B]^T [D][B] \cdot dV, \tag{3}$$

in which $[B]$ is a matrix relating element strains $\{\varepsilon\}$ to its nodal displacements $\{\Delta\}$, and $[D]$ is the material stiffness matrix, relating element stresses $\{\sigma\}$ and strains $\{\varepsilon\}$:

$$\{\sigma\} = [D]\{\varepsilon\} \tag{4}$$

The finite-element formulation thus requires the stress-strain relation of all component materials to be expressed in the form of Eq. 4; for an elastic

isotropic material of modulus E and Poisson's ratio ν under plane stress as shown in Fig. 2, for instance, Eq. 4 is represented by the classical Hooke's Law:

$$\begin{Bmatrix} \sigma_{xx} \\ \sigma_{yy} \\ \sigma_{xy} \end{Bmatrix} = \frac{E}{1-\nu^2} \begin{bmatrix} 1 & \nu & 0 \\ \nu & 1 & 0 \\ 0 & 0 & \frac{1-\nu}{2} \end{bmatrix} \begin{Bmatrix} \varepsilon_{xx} \\ \varepsilon_{yy} \\ \varepsilon_{xy} \end{Bmatrix} \tag{5}$$

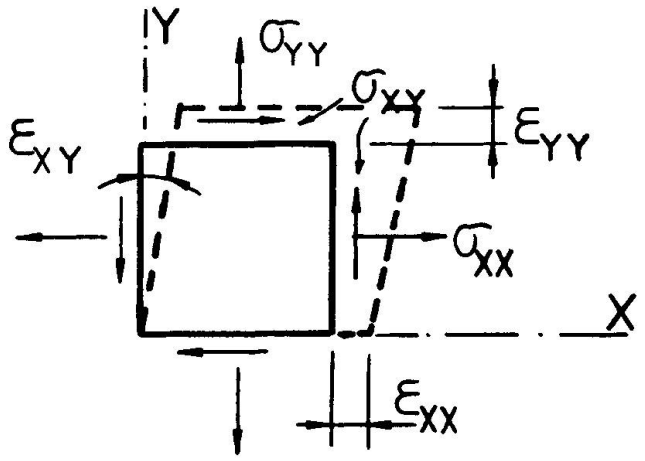

Fig. 2 Plane Element

As at the element level, the stiffnesses of the materials in parallel, as for instance that of concrete, $[D^C]$, and that of steel, $[D^S]$, in the reinforced concrete element shown in Fig. 3, can be superimposed:

$$[D] = [D^C] + [D^S] \quad . \tag{6}$$

The individual stiffnesses must be referred to a common coordinate system; matrix transformations may be required when the principal material directions deviate from each other; if, for instance, the reinforcing layer i along the U axis, of stiffness with respect to this axis

$$[D^i] = p^i E^S \begin{bmatrix} 1 & 0 & 0 \\ 0 & 0 & 0 \\ 0 & 0 & 0 \end{bmatrix}$$

makes an angle α with the reference axes as shown in Fig. 3, then its stiffness matrix $[D^S]$ with respect to the common axes X,Y is given by

$$[D^S] = [\lambda][D^i][\lambda^T] = p^i E^S \begin{bmatrix} \cos^4\alpha & \cos^2\alpha \sin^2\alpha & \cos^3\alpha \sin\alpha \\ \cos^2\alpha \sin^2\alpha & \sin^4\alpha & \cos\alpha \sin^3\alpha \\ \cos^3\alpha \sin\alpha & \cos\alpha \sin^3\alpha & \cos^2\alpha \sin^2\alpha \end{bmatrix} = p^i E^S [T] \tag{7}$$

p^i is the steel ratio A_s/bd, and E^S is the elastic modulus of the steel in the i-th layer; $[\lambda]$ is a matrix of direction cosines given, for instance, in Ref. 1, Eq. 4.15. The problem is now to determine appropriate stiffness matrices $[D^C]$ and $[D^S]$ for the many-faceted behavior of concrete and steel to be inserted into Eq. 6.

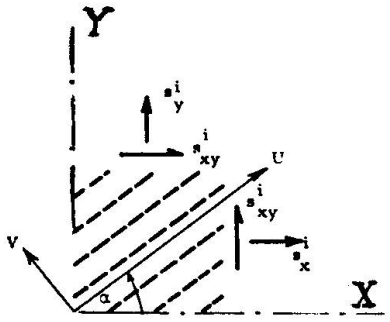

Fig. 3 Reinforcement Stresses

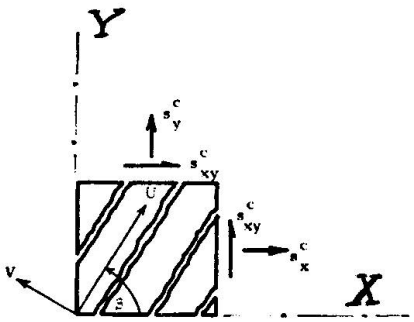

Fig. 4 Concrete Stresses in the Cracked Concrete

1.2 Reinforced Concrete Stiffness

1.2.1 Uncracked Concrete

Before cracking of the concrete, elastic isotropic behavior may be assumed at low stress levels; accordingly, Eq. 5, with E and ν representing the modulus and Poisson's ratio of the plain concrete, is appropriate.

At higher stress levels, non-linear behavior is conveniently expressed by separating the volumetric (hydrostatic, or octahedral normal) response, expressed by the bulk modulus K, and distortional (deviatoric, or octahedral shear) response, expressed by the shear modulus G; the $[D^C]$ matrix for plane stress is given in terms of K and G in Ref. 2 as

$$[D^C] = 4G \frac{3K+G}{3K+4G} \begin{bmatrix} 1 & \frac{3K-2G}{2(3K+G)} & 0 \\ \frac{3K-2G}{2(3K+G)} & 1 & 0 \\ 0 & 0 & \frac{3K+4G}{4(3K+G)} \end{bmatrix} \tag{8}$$

For K and G constant, the elastic relations of Eq. 5 result from Eq. 8; the non-linear behavior of the concrete requires variable tangent or secant moduli K and G; various formulations for these moduli are given in Refs. 3, 4, 5.

Compressive crushing of concrete has been represented using plasticity formulations without and with (6) strain hardening. Isotropic load history effects are formulated in the endochronic theory (7). Directional preference due to prior microcracking as well as post-peak compressive concrete behavior have been formulated (8, 9), and may become important under severe load histories.

1.2.2 Cracked Concrete (10)

Tensile cracking of the concrete will occur in a direction normal to the principal tensile concrete stress when this reaches the tensile cracking strength given, for instance, in Ref. 11. Thereafter a cracked element as shown in Fig. 4 may be visualized, capable of carrying only normal stresses parallel to the cracks:

$$\sigma^c_{uu} = E^c \varepsilon_{uu} \quad \text{or} \quad \begin{Bmatrix} \sigma_{uu} \\ \sigma_{vv} \\ \sigma_{uv} \end{Bmatrix} = E^c \begin{bmatrix} 1 & 0 & 0 \\ 0 & 0 & 0 \\ 0 & 0 & 0 \end{bmatrix} \begin{Bmatrix} \varepsilon_{uu} \\ \varepsilon_{vv} \\ \varepsilon_{uv} \end{Bmatrix} \tag{9}$$

Transformation from the U, V, to the X, Y axes, as discussed earlier in connection with Eq. 7 leads to the cracked concrete stiffness matrix

$$[D^c] = E^c \cdot [T] \; ; \tag{10}$$

the angle α in the [T] matrix should here be replaced by the angle β between the X and the U axes.

Under load histories, cracks in the concrete can successively open and close, as shown, for instance, in Fig. 5. Two sets of cracks at right angles to each other may also occur. These possibilities must be monitored in a step-by-step analysis, and the $[D^c]$ matrix adjusted to reflect the current state of each element.

Non-linear behavior of the cracked concrete can be taken into account by appropriate choice of variable moduli K and G in Eq. 8. Fully plastic response of the cracked concrete can be represented by setting $[D^c] = 0$.

This approach to concrete cracking does not try to predict crack spacing or crack width; the effect of the cracks is "smeared" over the entire element. The predicted crack pattern for a reinforced concrete panel obtained from a formulation as outlined, and shown in Fig. 6a (12) is intended to predict the extent of the cracked zone, and crack directions; the crack spacing is purely a function of the element size selected for analysis: the program indicates one crack through each element. The actual crack pattern observed in test, shown in Fig. 6b, illustrates this difference.

Attempts to predict actual crack spacings and widths have been made by running cracks between elements, rather than smearing them over the elements (13). Because this requires reformulation of the finite-element topology after each crack propagation, this approach does not appear suitable for the analysis of complete concrete structures.

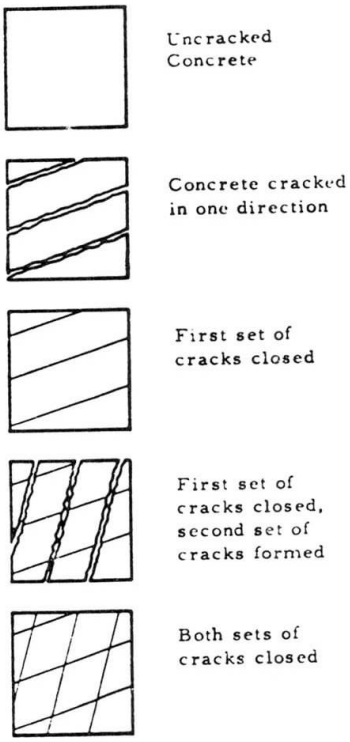

Fig. 5 Crack Modes

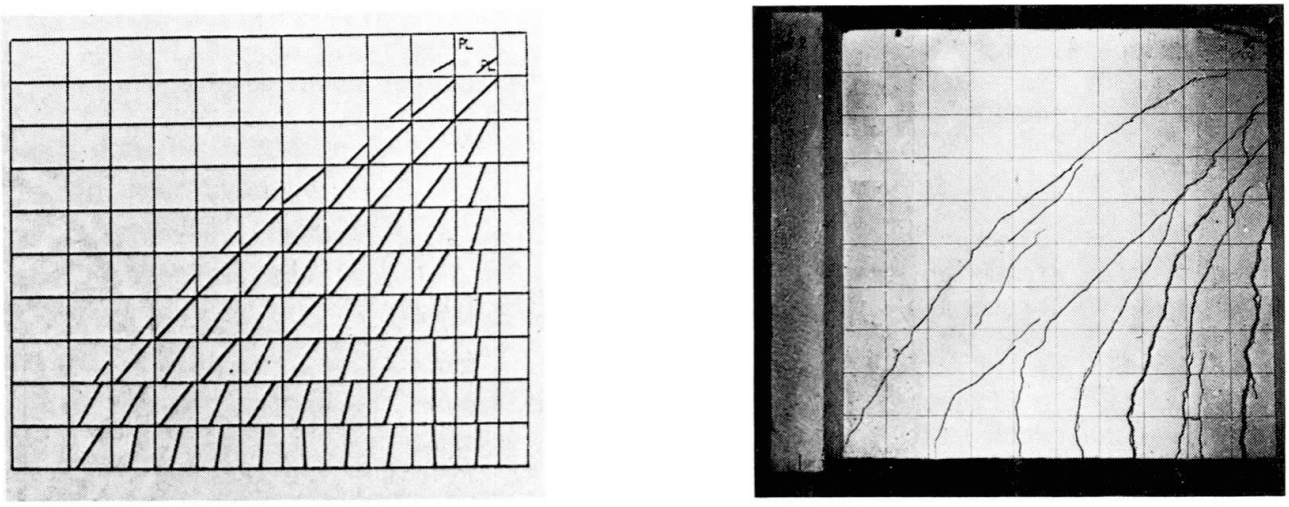

a, Predicted b, Observed

Fig. 6 Crack Pattern

1.2.3 Reinforcement

The case in which the steel in the i-th layer, making an angle α with the reference axes, acts elastically, has already been formulated in Eq. 7; when the plastic limit of this steel is reached, its stiffness vanishes: $[D^i] = 0$. Strain-hardening can also be represented by appropriate modification of Eq. 7. Elastic unloading and reloading of the steel requires monitoring of the steel strains and strain rate, and suitable adjustment of the matrix $[D^i]$.

1.3 Anisotropy of Reinforced Concrete (10)

The reinforcing layer i, represented by Eq. 7, of preferred direction α, as well as cracked concrete of preferred direction β, lead to an anisotropic stiffness matrix [D] when inserted into Eq. 6; this anisotropy will cause deviation of the axes of principal stress and strain within the element: for instance, pure uniaxial tension stress will cause shear distortion of the reinforced concrete, as discussed further below. The degree of anisotropy depends on the reinforcing as well as prior cracking of the concrete.

As an example, we consider the element of previously uncracked concrete and x and y reinforcing of ratios $p_x = 4 \cdot p_y$, as shown in Fig. 7a, inclined at an angle $\alpha = 30^o$ with the principal stress directions (10). Fig. 7b plots the deviation of crack direction, δ, from the principal stress axes, using Eqs. 7 and 6. It is seen that for these conditions, even a small inequality of the principal stresses will cause a great deviation of the cracks from both the principal stress axes, and the directions of reinforcing.

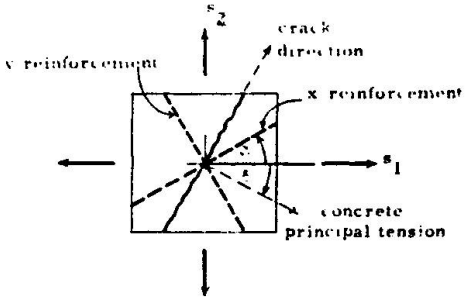

Fig. 7a Deviation of Crack Direction from Total Principal Stress Direction Caused by Reinforcement

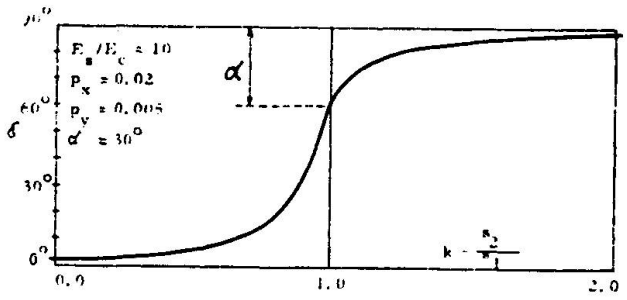

Fig. 7b Effect of Stress State on the Deviation of Concrete Principal Directions

1.4 Experimental Correlation (12)

To check the strains and cracks predicted by Eqs. 4 and 6 experimentally, we refer to the results of a famous test series by Peter (14). Fig. 8 shows the panels tested in uniaxial tension; they contained a grid of equal reinforcing in orthogonal directions, at angles ranging from 0° to 40° with the principal stress direction. Fig. 9 shows the load-extension relations plotted for various values of α; the dashed lines represent predicted response using Eqs. 4 and 6, the solid curves are the measured test results. The actual behavior

beyond cracking shows much greater stiffness than predicted, and none of the discontinuity associated with cracking predicted by theory. This tension-stiffening is due to the bond between steel and concrete between discretely spaced cracks; under increasing load, this bond gradually deteriorates, leading to better agreement between theory and measurement at large extensions.

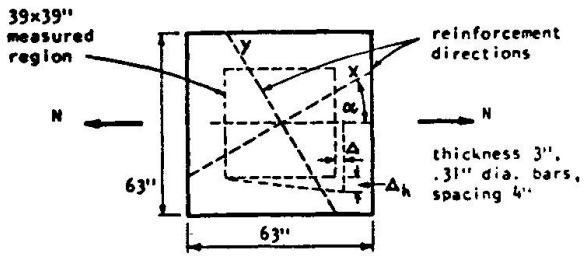

Fig. 8 Peter's Test Panel Subjected to Uniaxial Tension

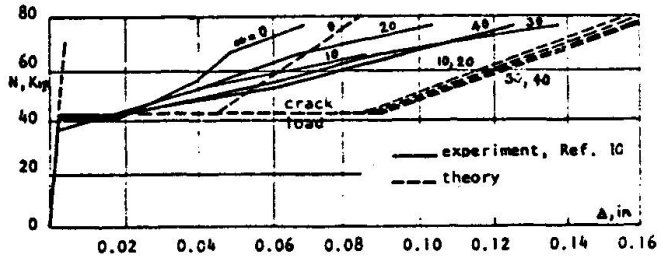

Fig. 9 Load-Extension Relationships

It follows from this observation that a more realistic formulation of the bond-slip behavior between steel and concrete is necessary for prediction of the response of the response of concrete structures with tension cracks. Such formulations will be outlined further on.

The transverse displacement, Δ_h, shown in Fig. 8, is a measure of the shear distortion of the anisotropic panel under uniaxial tension. Fig. 10 shows the predicted, and measured, shear distortion for various reinforcement inclinations α for one load level. For values of less than 30°, the actual shear strain is much less than predicted by the theory which disregards any shear resistance of the crack, as in Eq. 9; in fact, aggregate interlock and dowel action of the bars contribute considerable shear stiffness across cracks, which is indicated by the shaded area of Fig. 10.

It can be concluded that the crack behavior is in fact much more complicated than shown in Figs. 4 or 5, and represented by Eq. 9; these interface shear transfer effects, to be discussed later, should obviously be included in more refined analyses.

2. INTERFACE SHEAR TRANSFER

2.1 Crack Behavior

Fig. 10 shows that the elementary approach which neglects any ability of a concrete crack to transmit stresses can lead to sizable error. In fact, the rough surfaces of narrow cracks can transfer shear stresses through aggregate interlock, which diminishes as the crack becomes wider under further loading.

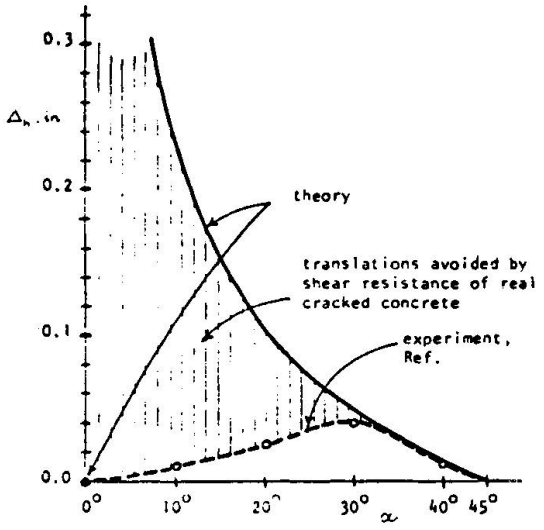

Fig. 10 Effect of Reinforcement Direction on the Transverse Displacement at Load N = 77 Kips

Further, the asperities of the rough crack surfaces will tend to cause a spreading or dilatation of the crack upon sliding, as shown in Fig. 11. When this dilatation is constrained either by surrounding portions of the structure and its supports, or by reinforcing bars crossing the crack, compression results in the concrete which can strengthen the structure but may also under some conditions cause over-stress in the reinforcing steel in tension (15).

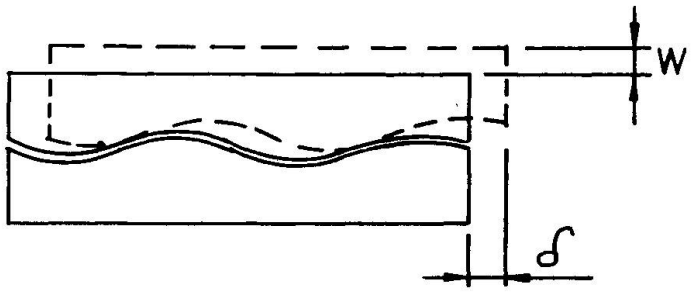

Fig. 11 Crack Displacements

These effects may thus become important under some conditions, particularly under non-proportional load histories in which the principal stress direction changes so that cracks formed initially due to excessive tension become planes of maximum shear under subsequent loads. This has been investigated in the case of nuclear containment vessels which may be under internal pressure followed by earthquake shears (16, 17). It should be realized, however, that these are secondary effects and that many successful analyses, particularly

under proportional loadings, have been performed without considering interface shear transfer.

The detailed behavior of cracks may be considered in two ways: either by looking at each single crack "under a magnifying glass": the shear transfer and dilatation are expressed quantitatively as properties of a joint element which models the crack; this requires knowledge of the location and extent of each crack, something usually not known a priori; further crack propagation requires rearrangement of the element topology from load step to load step. Accordingly, this approach is mainly useful when the safety of a distressed structure, with well-defined existing cracks, is to be determined.

Alternately, when general cracking of a region of the concrete structure may be expected, its shear resistance may be averaged and included as a reduced shear modulus in the material stiffness matrix for the elements representing the cracked region; this approach is clearcut and economical in calculations.

Both of these approaches will be outlined in the following.

2.2 Finite Joint Element

Fig. 12a shows a well-defined crack modelled by a series of joint elements, and Fig. 12b shows one such element in detail; normal and shear stresses, σ and τ, lead to dilatation w and slip δ; these quantities are related by the stiffnesses k_{ij}:

$$\begin{Bmatrix} \sigma \\ \tau \end{Bmatrix} = \begin{bmatrix} k_{11} & k_{21} \\ k_{21} & k_{22} \end{bmatrix} \begin{Bmatrix} w \\ \delta \end{Bmatrix} \tag{11}$$

The element stiffness k_{ij} are, in general, nonlinear functions of stress and displacement levels and rates, as well as prior load histories. Non-zero off-diagonal terms indicate coupling between normal and shear quantities: k_{12} indicates dilatation under slip, which, as previously discussed, can be expected. However, k_{21} indicates sliding under normal stress, which is unlikely. Thus, an unsymmetric stiffness matrix results which will be upsetting not only to the classically-trained analyst, but also to the typical finite-element program.

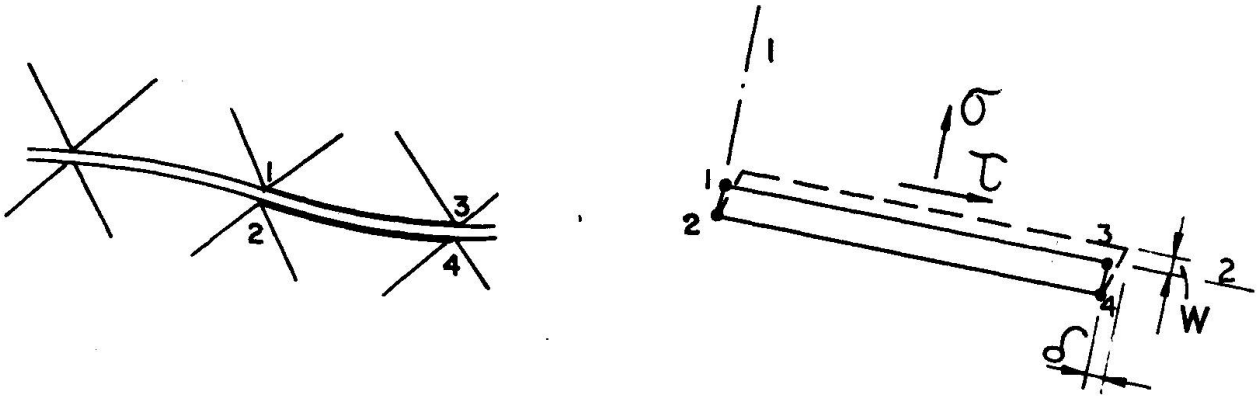

a. Element Grid b. Joint Element

Fig. 12. Joint Element

Little is known about appropriate values for the stiffnesses k_{ij} in Eq. 11. Only the shear, or sliding, stiffness k_{22} has been investigated by a number of researchers (16, 18, 19); in general, shear stress-slip curves appear linear for relatively low stress levels, with diminishing stiffness as cracks get wider; Fig. 13 shows values for the stiffness k_{22} for different crack widths, as obtained in different studies. It might be expected that for higher shear displacements, frictional behavior, analogous to perfect plasticity, might prevail; yet further, the asperities might be sheared off, with consequent loss of shear resistance, as might also prevail under load cycles.

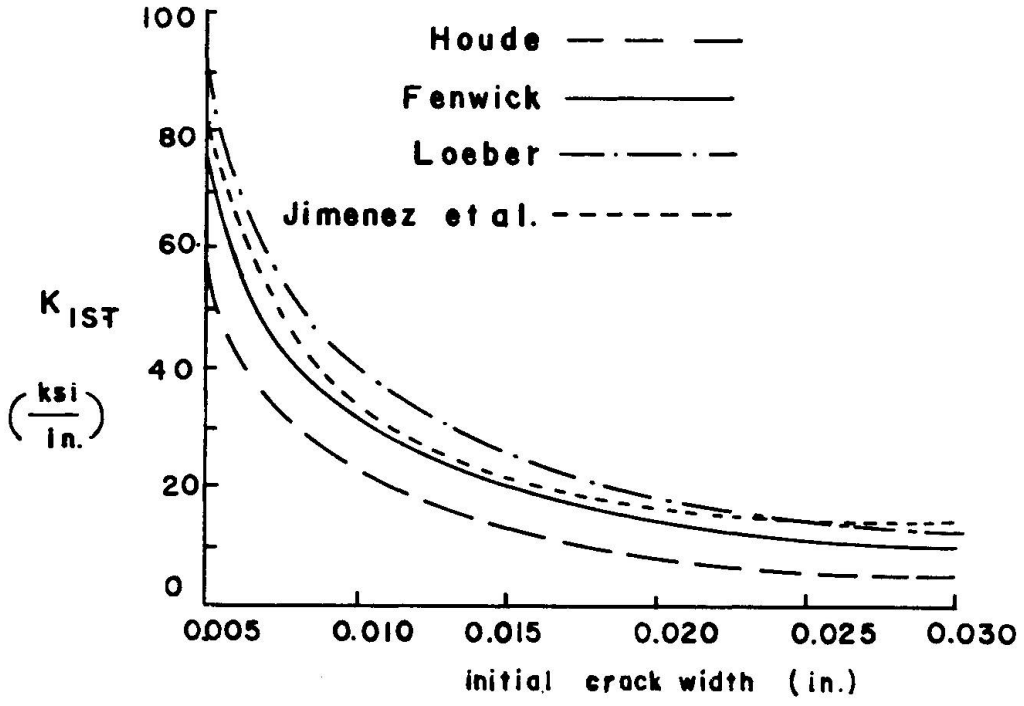

Fig. 13. Crack Shear Stiffness - Crack Width Relation (17)

The normal stress-normal displacement stiffness is strongly sign-dependent: no resistance will be offered to crack opening, while crack closing will have k_{11} = 0 as long as the crack is open, followed by k_{11} proportional to the plain concrete modulus after crack closure. Clearly, any step-by-step program must monitor both current crack widths as well as sense of the displacement.

The coupling term k_{21} is zero, as discussed. No values for k_{12} have been found in the literature, but are badly needed since dilatation during crack slip may contribute importantly to the performance of the cracked structure.

It should be noted that crack displacements are not strains; accordingly, the stiffness k_{ij} have units of F/L^3. The width of the joint element of Fig. 12b may in fact be zero, with opposing joints of identical location. In any case, nodes will have to be so arranged as to allow superposition of the concrete and steel elements for analysis.

2.3 Overall Cracking

In practice, location and nature of any single crack will usually be unknown, and it may become more practical to base the prediction of crack effects on an overall crack pattern as shown in Fig. 14. The degradation of in plane behavior is reflected mainly in the decrease of the shear modulus $G_c = \frac{E}{2(1-\nu)}$ of the plain concrete shown in k_{33} in Eq. 5. This decrease is strongly dependent on crack width and spacing and thus on the degree of reinforcing.

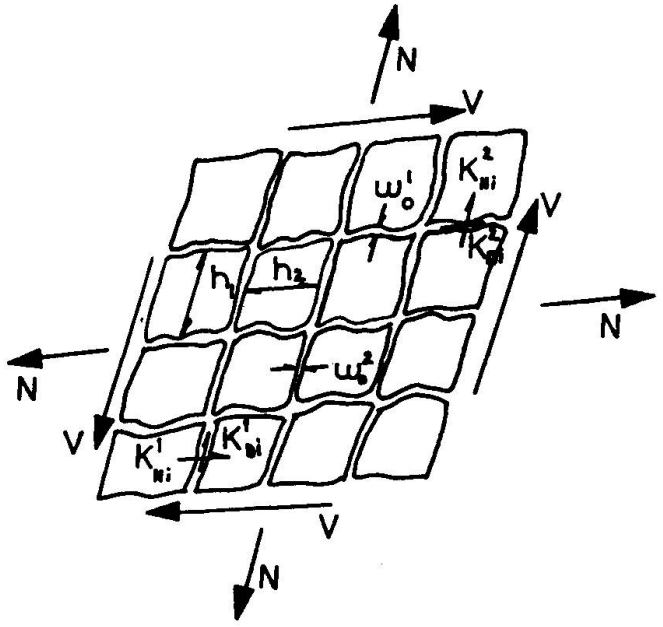

Fig. 14. Generally Cracked Element (17)

The reduced shear modulus G_{cr} or the cracked concrete is given in Ref. 17 as

$$G_{cr} = \left[\frac{1}{h_1\left(\frac{K_N^1}{\beta^1} + K_D^1\right)} + \frac{1}{h_2\left(\frac{K_N^2}{\beta^2} + K_D^2\right)} + \frac{1}{G_c} \right]^{-1} \qquad (12)$$

in which h_1 and h_2 are the expected crack spacings in each crack direction, K_N and K_D are transverse and dowel stiffnesses of the reinforcing, and β represents the effect of aggregate interlock, and is thus a function of the crack width. The three terms in Eq. 12 are nothing more than the effects of the shear displacements due to the cracks in Directions 1, and 2, and those of the uncracked concrete between cracks, respectively.

Figure 15 (20) shows the reduction of shear modulus due to cracking which has been used by different analysts. The range is considerable, from 50 percent to only 10 percent for very wide cracks.

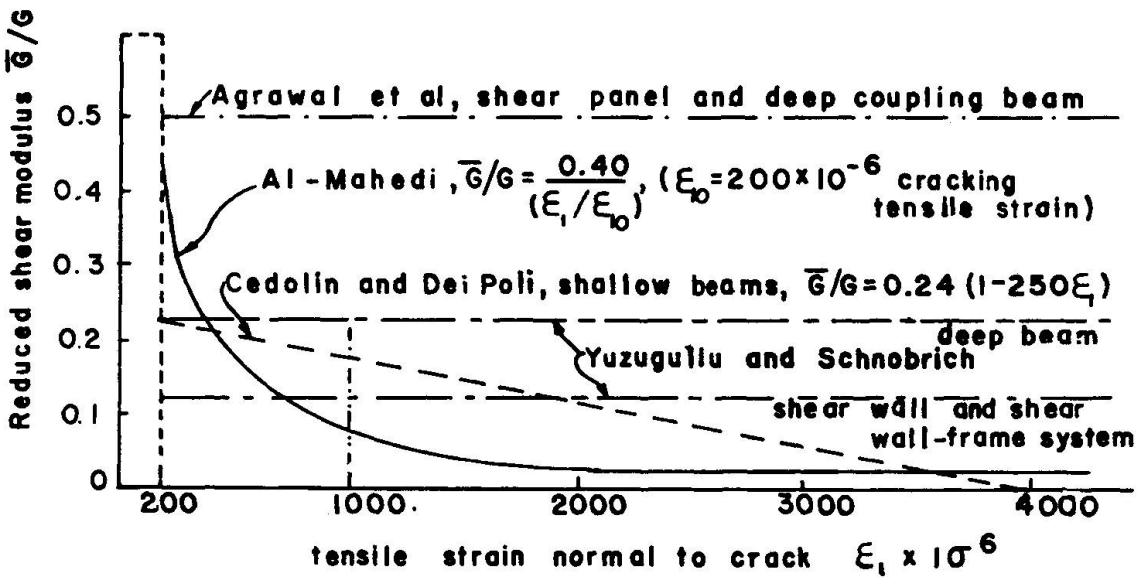

Fig. 15. Shear Stiffness Reduction in Cracked Concrete (20)

Eq. 12 does not consider the important effect of dilatation due to slip of cracks, nor the directional effects of cracking. A more elaborate formulation of the degradation of the concrete due to regularly-spaced cracks which includes both of these effects is presented in Ref. 15. A great deal of laboratory work remains to be done before all experimental parameters necessary for implementation of these formulations are available.

3. BOND SLIP

3.1 General

Fig. 9 showed that the bond between steel and concrete has a considerable effect on the structure behavior after cracking. In fact, if perfect bond without slip is assumed, as in classical reinforced concrete theory, then cracks would not be able to open at all. It follows that rational prediction of crack widths requires knowledge of bond behavior between reinforcing and concrete.

Nevertheless, bond-slip and bond degradation is in many analyses only of secondary importance, and may not affect overall structure behavior significantly, specially for monotonic loading cases.

3.2 Force Transfer and Concrete Cracking

Assuming continuous action along the reinforcing bar, statics of longitudinal forces on a bar element of length dx and perimeter Σ_0 requires that

$$u = \frac{1}{\Sigma_0} \cdot \frac{dP}{dx} \tag{13}$$

that is, the bond stress u is proportional to the rate of change of the axial bar force P. Using this relation, Fig. 16 shows schematically the relation between bond stress, bond slip, crack width, and crack spacing.

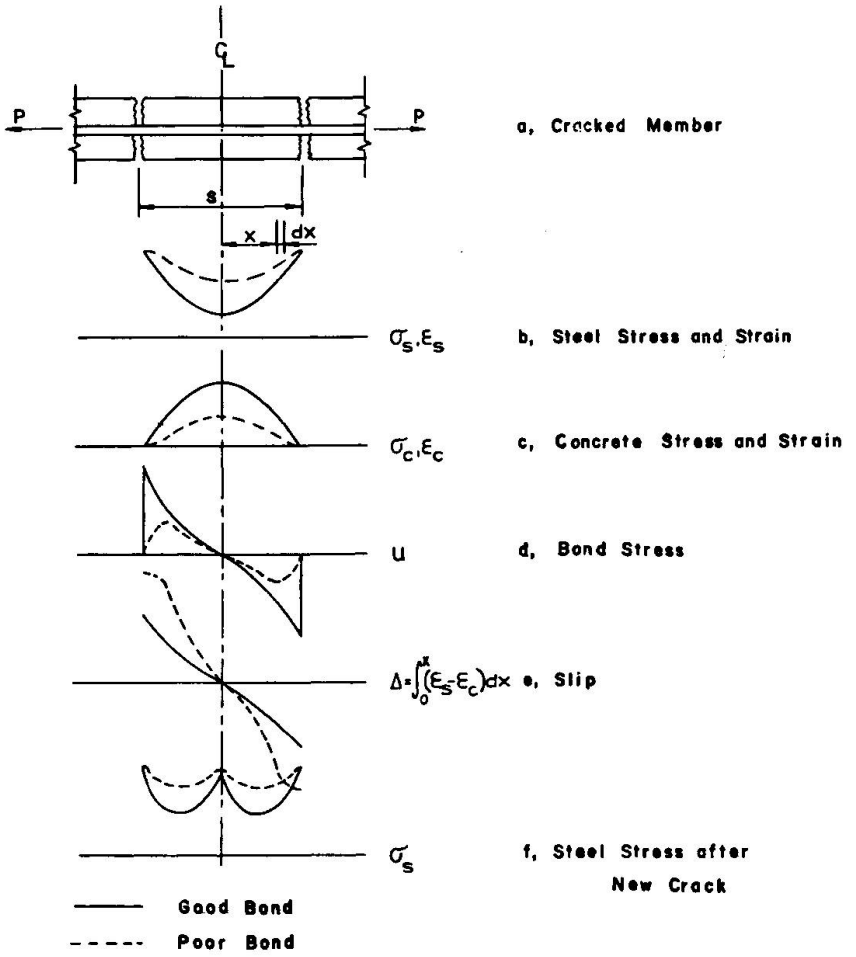

Fig. 16
Relations between Stresses, Bond Slip, and Cracking.

Fig. 16a depicts a portion of a reinforced concrete member between two existing cracks caused by the tension force P in the bar. The steel stress shown in Fig. 16b varies from a maximum at the cracks to a minimum at the uncracked section midway between the cracks. The concrete stress must then pick up the balance of the tension force as shown in Fig. 16c. According to Eq. 13, the bond stress variation must be as shown in Fig. 16d, with a sharp gradient in the vicinity of the cracks.

Under increasing force P, the concrete stresses of Fig. 16c increase until their maximum at the midpoint reaches the tensile strength, at which instance the concrete ruptures, causing a new crack midway between the earlier cracks. From the relations between the bar stresses of Fig. 16b and the bond stresses of Fig. 16d, it follows that the quality of bond strongly affects the occurrence of subsequent cracks. The better the bond, the closer the crack spacing and the narrower the cracks, a well-known fact. After occurrence of the next crack, the steel stress is distributed as in Fig. 16f, and the next cycle of crack formation begins. The nature of this process has been discussed by Broms (21).

Corresponding to the steel and concrete stresses shown in Figs. 16b and 16c, there will be steel and concrete strains ε_s and ε_c; stresses and strains may be proportional for elastic materials, or non-proportional for nonlinear material

behavior. According to this simplified approach, the slip can be found by integrating the difference of steel and concrete strains, starting from the centerline; the crack width should then be equal to the total slip between cracks. In fact, the situation is more complex because a uniaxial analysis as presented here cannot account for the actual three-dimensional strains and crack formation. This real behavior can be represented by a finite-element formulation as outlined in the next section.

3.3 Modeling of Bond Behavior

Bond slip can be modeled by introduction of an appropriate discrete bond-link element, shown in Fig. 17 (13). The spring, of modulus k, represents the resistance offered to slip Δ by the bond stress u:

$$k = \frac{du}{d\Delta} \quad ; \tag{14}$$

the magnitude of this stiffness will be discussed next.

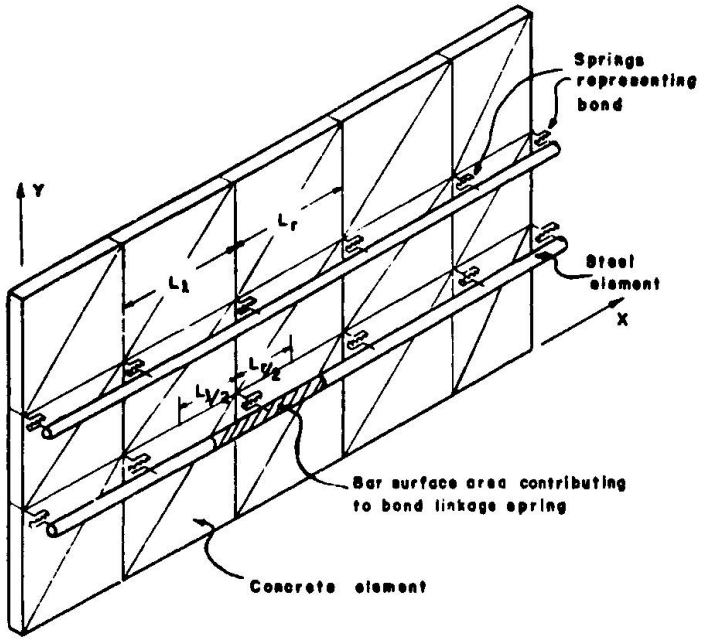

Fig. 17. Bond-Link Element (26)

The splitting effect of the steel bar could be represented by additional degrees of freedom of the link element, but because almost nothing is known about these radial forces, we will not consider them any further.

With sufficient number of these bond-link elements, and knowledge of their stiffness k, the interface behavior between steel and concrete can be modeled.

Experimental determination of the slip resistance k is difficult, and little actual information covering a full range of conditions is available. Fig. 18

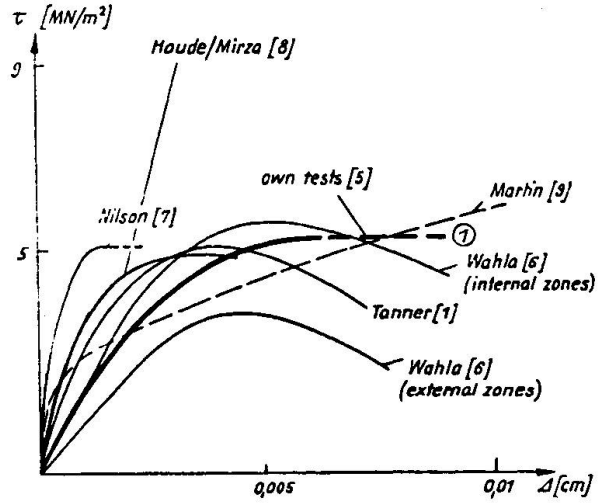

Fig. 18. Bond Stress-Slip Relations (22)

(22) shows the staggering variation of results obtained by different investigators.

Among the more comprehensive tests (covering, however, only one bar size and concrete type) are those of Nilson (23), performed on a specimen as in Fig. 16a, which represents the situation between two existing cracks. The resulting bond stress-slip curves of Fig. 19, which are highly non-linear, indicate that the stiffness k, obtained as the slope of these curves, depends on the distance from the crack faces; it is thus not a unique property of the element, but depends on its neighborhood. This is quite at variance with the basic concepts of finite-element analysis.

Bond-slip under load cycles or load reversals as under seismic shocks can lead to severe bond degradation (24). Morita and Kaku (25) have obtained bond stress-slip relations under cycles of load reversal: Fig. 20a shows one of their typical load cycles which reveals ranges of bearing of the bar ribs against the concrete, as well as frictional resistance. Shipman (26) idealized this behavior for purposes of finite-element analysis as shown in Fig. 20b. Good results were obtained with this model.

Our understanding of these phenomena is just in its infancy.

3.4 Tension Stiffening

Just as in the case of crack behavior, bond can be modeled either by "looking through the magnifying glass", as we have just done, or by taking an averaging approach. The latter has been taken by introducing the concept of tension-stiffening (27). The variable tensile resistance of the concrete surrounding the bar, shown in Fig. 16c, ranging from nil at the crack to full effectiveness at the midpoint between cracks, is averaged by assigning a post-peak range to the tensile concrete stress-strain relation, as shown in Fig. 21. The effectiveness of this concept has been demonstrated in several analyses (28), and has also been extended to the multiaxial case (29).

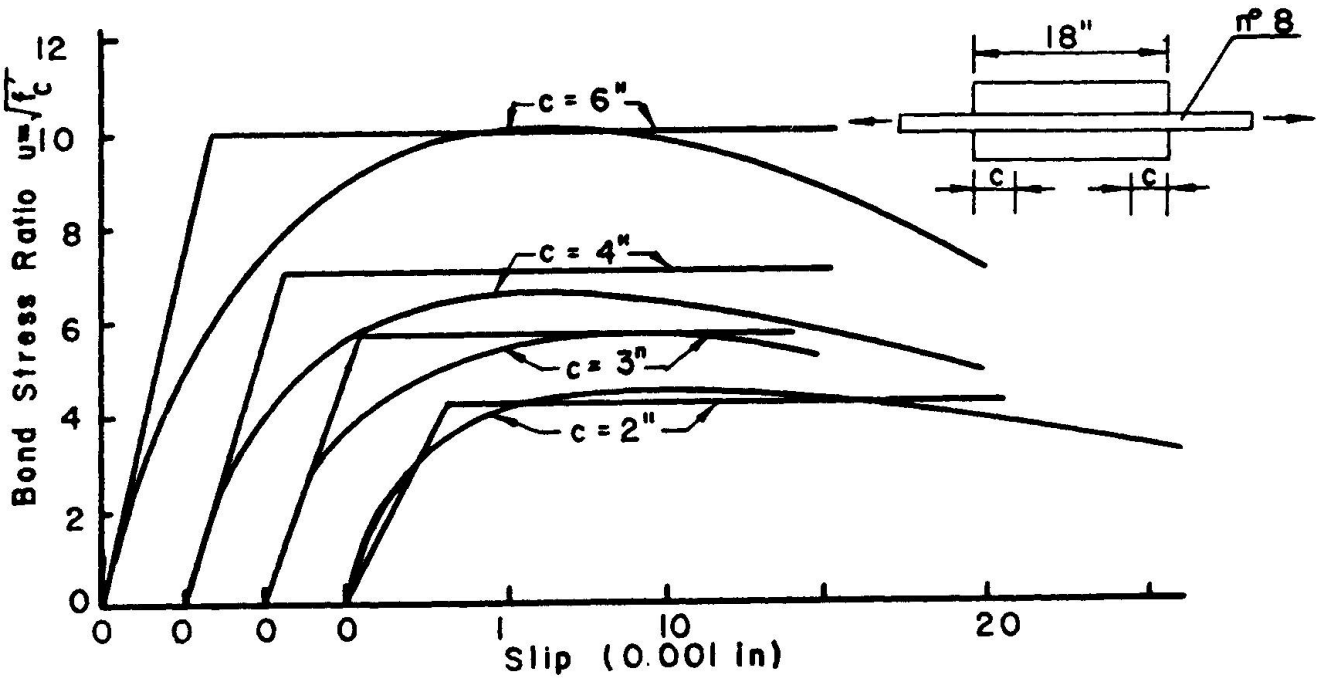

Fig. 19. Bond Stress-Slip Relations of Nilson (23)

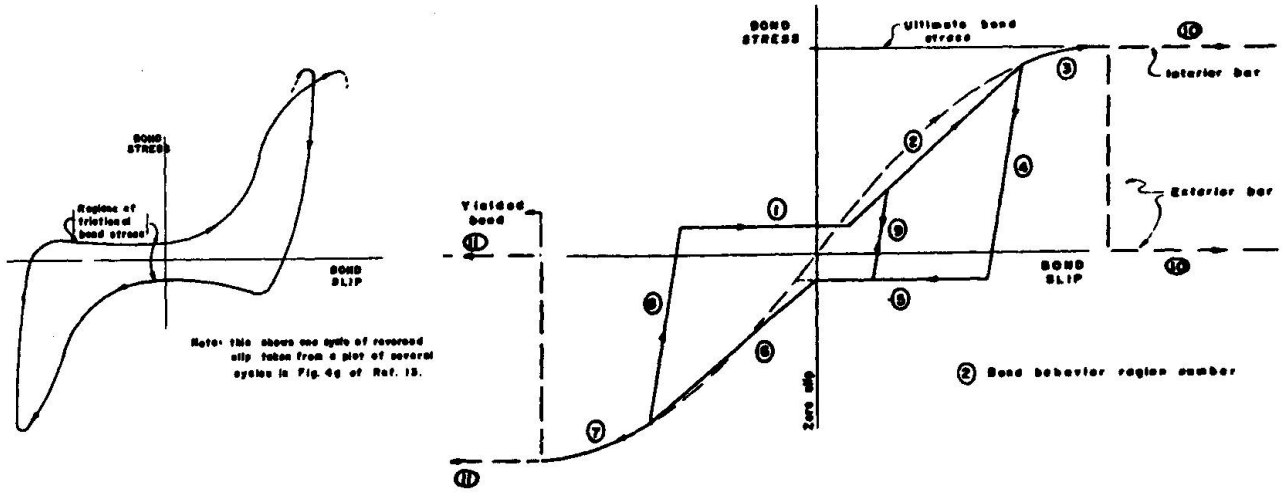

a, Actual Behavior b, Idealization

Fig. 20. Bond Stress-Slip Relations under Load Cycles

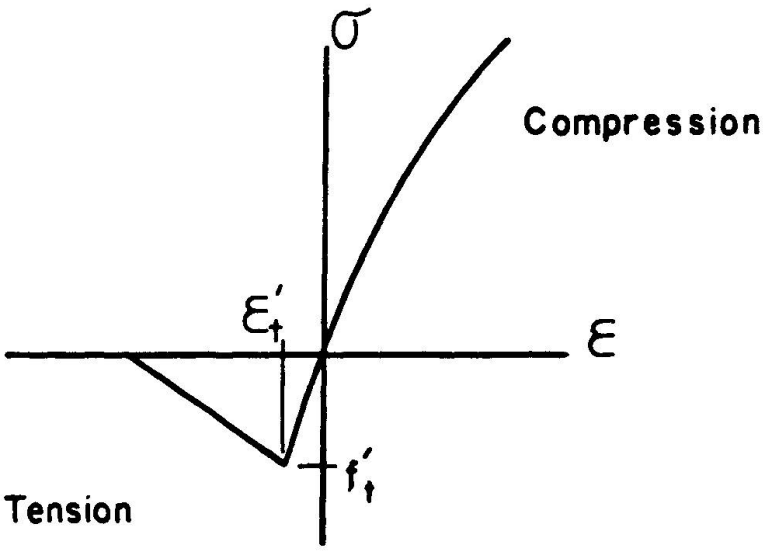

Fig. 21. Concrete Behavior for Tension-Stiffening

4. MODELING PROBLEMS OF CONCRETE STRUCTURES

4.1 Some Unknown Factors

Lastly, we wish to cast a critical eye on the feasibility of realistic modeling of the behavior of reinforced concrete structures.

Only some of the many factors which influence the structural performance have been considered in the foregoing, and most of these have been of non-linear character. The current state of the computer art is such that any non-linear analysis must be considered of developmental nature, and therefore beyond the realm of professional engineering practice. A level head must be preserved regarding the feasibility of realistic analyses under the constraints of office practice.

Looking beyond the basics which have been covered, we wish to draw attention to just a few of the many additional factors which may affect the performance of concrete structures as significantly as those discussed:

1. Time-dependent Behavior of Concrete: Concrete creeps and is likely to affect deformations and cracking.

2. Temperature Effects: Not only seasonal or daily temperature variations, but specially those occurring due to curing of the weak concrete during construction, are quite likely to cause high stresses and cracking.

3. Load Histories: The sequence of load application on real structures during their construction and useful life is quite different from the monotonic loading to failure usually applied in the laboratory. We know very little about the response of plain concrete and its crack- and steel interfaces under general load histories.

Obviously, much remains to be done before we can claim the power to make valid predictions of the response of real structures to real lifetime conditions.

4.2 Case Study

The reinforced concrete panels mentioned earlier (12) showed excellent correlation between predicted and observed behavior under monotonically increasing loads to failure, as shown, for instance, in Fig. 6. However, when subjected to load cycles, any inflated expectations were quickly punctured: as shown in Fig. 22, no correlation at all seemed to exist between analysis and experiment in such cases; actual deformations were larger than predicted by an order of magnitude.

In searching for reasons for these discrepancies, the following simplifications in the analysis were considered:

1. Bond slip had been neglected.
2. Degradation of plain concrete under high stress cycles had been neglected.
3. Simultaneous crack opening in two directions had been neglected.
4. Effect of debris entering open crack upon crack closing had been neglected.
5. Creep of concrete had been neglected.

Of these five cited factors, comparative analyses were performed including No. 1 (26) and No. 2 (9). Fig. 23 summarizes the findings for the very restricted case of one half load cycle: about one third of the discrepancy between calculated and observed behavior can be ascribed to neglect of bond deterioration, the remainder to degradation of the plain concrete. The effect of the other approximations has not been studied.

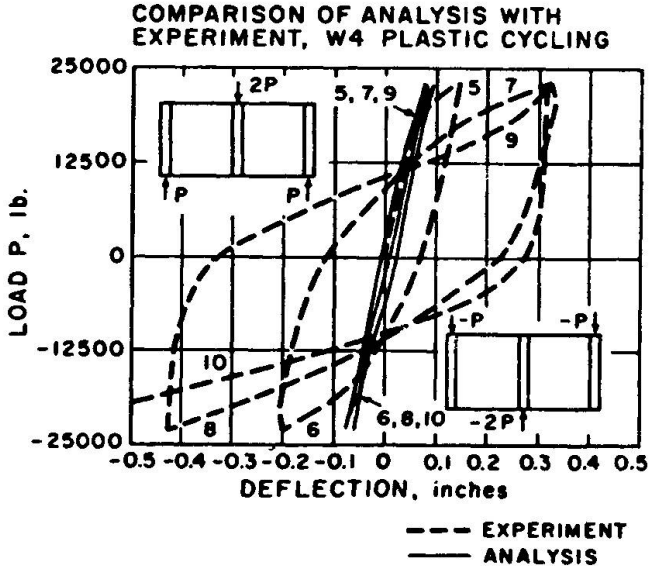

Fig. 22 Predicted and Actual Load-Deflection Curves for Reinforced Concrete Panel under Load Cycles (12)

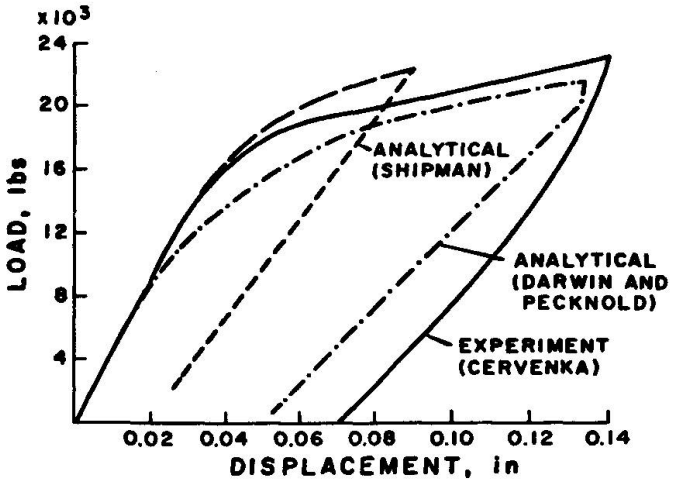

Fig. 23 Results of Two Analyses Compared with Experiment (26)

4.3 Conclusions

Reinforced concrete structures under realistic loading and use conditions are subjected to a great number of complex influences, only a few of which have

been studied in detail, The inclusion of most of these factors appears quite impossible in any routine analysis of real structures.

We do not at this time have much idea of the relative importance of these different effects under specified conditions of use. A systematic investigation of different influences, with the aim of establishing a list of priorities for specific cases, appears useful to achieve the required compromise between reality and simplicity which underlies the engineering approach.

ACKNOWLEDGEMENTS

The major portion of this report was written while the author was Senior Fellow of the Alexander von Humboldt-Foundation, Bonn, Germany, and on sabbatical leave from the University of Colorado, Boulder. Thanks are due for this financial support, as well as to the Technical University of Darmstadt, Germany, and to Professor Gerhart Mehlhorn, for their hospitality.

REFERENCES

1. Zienkiewicz, O.C., "The Finite Element Method in Engineering Science," 2nd Ed., McGraw-Hill, London, 1971.

2. Kupfer, H.B., and K.H. Gerstle, "Behavior of Concrete under Biaxial Stresses," Proc. A.S.C.E., Jul. E.M.D., Vol. 99, No. EM4, August 1973.

3. Cedolin, L., Y.R.J. Crutzen, S. Dei Poli, "Stress-Strain Relationship and Ultimate Strength of Concrete under Triaxial Loading Conditions," Proc. A.S.C.E., Jul. E.M.D., Vol. 103, No. EM3, June 1977.

4. Kotsovos, M.D., and J.B. Newman, "Generalized Stress-Strain Relations for Concrete," Proc. A.S.C.E., Jul. E.M.D., Vol. 104, No. EM4, August 1978.

5. Gerstle, K.H., H. Aschl, et al., "Behavior of Concrete under Multiaxial Stress States," Proc. A.S.C.E., Jul. E.M.D., 1980.

6. Chen, W.F., "Constitutive Equations for Concrete," Rept. I.A.B.S.E., Vol. 28, Colloquium Kopenhagen, 1979.

7. Bazant, Z.P., and P.D. Bhat, "Endochronic Theory of Inelasticity and Failure of Concrete," Proc. A.S.C.E., Jul. E.M.D., Vol. 102, No. EM4, August 1979.

8. Liu, T.C.Y., A.H. Nilson, F.O. Slate, "Biaxial Stress-Strain Relations for Concrete," Proc. A.S.C.E., Jul. Struct. Div., Vol. 98, No. ST5, May 1972.

9. Darwin, D., and D.A. Pecknold, "Analysis of R.C. Shear Panels under Cyclic Loading," Proc. A.S.C.E., Jul. Struct. Div., Vol. 102, No. ST2, February 1976.

10. Cervenka, V., and K.H. Gerstle, "Inelastic Analysis of Reinforced Concrete Panels: Theory," Pubs. I.A.B.S.E., Vol. 31-II, 1971.

11. Kupfer, H.B., H.K. Hilsdorf, H. Ruesch, "Behavior of Concrete under Biaxial Stress," Jul. A.C.I., Vol. 66, No. 8, August 1969.

12. Cervenka, V., and K.H. Gerstle, "Inelastic Analysis of Reinforced Concrete Panels: Experimental Verification and Application," Pubs. I.A.B.S.E., Vol. 32-II, 1972.

13. Ngo, D., and A.C. Scordelis, "Finite Element Analysis of Reinforced Concrete Beams," Jul. A.C.E., Vol. 64, No. 3, March 1967.

14. Peter, J., "Zur Bewehrung von Scheiben und Schalen ...," Dr.-Ing. Dissertation, T.H. Stuttgart, 1964.

15. Bazant, Z.P., and T. Tsubaki, "Friction-Dilatancy Model for Cracked Reinforced Concrete," Struct. Engin. Report No. 79-8/640f, Dept. of Civil Engin., Northwestern Univ., Evanston, Ill., August 1979.

16. Jimenez, R., P. Gergely, R.N. White, "Shear Transfer across Cracks in Reinforeced Concrete," Report No. 78-4, Department of Structural Engineering, Cornell Univ., Ithaca, N.Y., August 1979.

17. Buyukozturk, O., J.J. Connor, P. Leombonni, "Research on Modeling Shear Transfer in Reinforced Concrete Nuclear Structures," Proc. S.M.I.R.T., Berlin, Germany, August 1979.

18. Walraven, J.C., E. Vos, H.W. Reinhardt, "Experiments on Shear Transfer in Cracked Concrete," Proc. I.A.S.S. Symposium, Darmstadt, Germany, July 1978.

19. Fenwick, R.C., and T.O. Pauley, "Mechànism of Shear Resistance in Concrete Beams," Proc. A.S.C.E., Jul. Struct. Div., Vol. 94, No. ST10, Oct. 1968.

20. Al-Mahaidi, R.S.H., "Nonlinear Finite Element Analysis of Reinforced Concrete Deep Members," Report No. 79-1, Dept. of Struct. Engin., Cornell University, January 1979.

21. Broms, B.B., "Technique for Investigation of Internal Cracks in Reinforced Concrete Members," Jul. A.C.I., Vol. 62, January 1965.

22. Dörr, K., "Bond Behavior of Ribbed Reinforcement under Transversal Pressure," Proc. I.A.S.S. Symp. Darmstadt, Germany, July 1978.

23. Nilson, A.H., "Bond Stress-Slip Relation in Reinforced Concrete," Struct. Eng. Dept. No. 345, Cornell University, December 1971.

24. Bresler, B., and V. Bertero, "Behavior of Reinforced Concrete under Repeated Loads," Proc. A.S.C.E., Jul. Struct. Div., Vol. 94, No. ST6, June 1968.

25. Morita, S., and T. Kaku, "Local Bond Stress-Slip Relationship under Repeated Loading," Proc. I.A.B.S.E. Symp., Lisbon, Portugal, Sept. 1973.

26. Shipman, J.M., and K.H. Gerstle, "Bond Deterioration in Concrete Panels under Load Cycles," Jul. A.C.E., Vol. 76, No. 2, February 1979.

27. Scanlon, A. and D.W. Murray, "Time-Dependent Deflections of Reinforced Concrete Slabs," Proc. A.S.C.E., Jul. Struct. Div., Vol. 100, No. ST9, Sept. 1974.

28. Gilbert. R.I., and R.F. Warner, "Tension-Stiffening in Reinforced Concrete Slabs." Proc. A.S.C.E., Jul. Struct. Div., Vol. 104, No. ST12, December 1978.

29. Geistefeld, H., "Multiaxial Tension-Stiffening Constitutive Relations for Concrete," Proc. I.A.S.S. Symposium, Darmstadt, Germany, July 1978.

Leere Seite
Blank page
Page vide